VILNIUS UNIVERSITY
FACULTY OF CHEMISTRY AND GEOSCIENCES
INSTITUTE OF CHEMISTRY
DEPARTMENT OF INORGANIC CHEMISTRY

Faryal Assad
Degree programme Pharmaceutical Chemistry
Master thesis

Calcium Hydroxyapatite: Comparative Study of Synthesis Methods and Fabrication of Composite with Eugenol

Scientific advisers
Prof. Habil. Dr. Aivaras Kareiva
Assoc. Prof. Dr. Živilė Stankevičiūtė

_____
(permission to defend, date, signature)
Scientific consultant:
Dr. Maab Abdulsamad Ahmed Elsheikh

Date of submission _____
Registration No. _____

Vilnius 2025

Table of Contents

INTRODUCTION

Calcium hydroxyapatite ($Ca_{10}(PO_4)_6(OH)_2$; CHA) is a naturally occurring mineral that serves an essential function in the robust composition of human bones and dentition. Due to its chemical composition and structural similarity to hard tissues, it is a vital material for biomedical applications. CHA is widely used in the fields of bone grafts [1], dental implants [2], and tissue engineering scaffolds [3], where its excellent biocompatibility and bioactivity [4], as well as its ability to be integrated with the living tissue, provide benefits for medical treatment.

CHA can be synthesized by various methods, including precipitation, sol-gel, and hydrothermal techniques. Each of these methods offers unique advantages in controlling the material's properties, such as particle size, morphology, and crystallinity, which significantly influence its performance in specific applications [5]. For instance, materials with optimized crystallinity and morphology are more suitable for bone repair and tissue regeneration [6,7]. Recent advancements in synthesis methods focus on tailoring these characteristics to expand the functional properties of hydroxyapatite and increase its utility in medical treatments [8].

A promising strategy to increase the multifunctional abilities of hydroxyapatite is the development of composites with biologically active compounds. Eugenol is a phenolic compound that is obtained primarily from clove oil and is well known for possessing antimicrobial, anti-inflammatory, and analgesic properties [9,10]. Integrating eugenol into hydroxyapatite can lead to multifunctional materials that combine the mechanical and structural properties of hydroxyapatite with the therapeutic properties of these compounds [12]. They are promising composites used in dentistry and orthopedics due to the surface functionality resulting in infection prevention, enhanced healing, and long-term drug incorporation [13,14]

The main objective of this work is to carry out a comparative study of the different synthesis methods for CHA, as well as to prepare its composites with eugenol. This study explores the structural, chemical, and antibacterial properties of these materials to assess their potential applicability in medicine and dentistry. [15]

Objectives

The following tasks were set to achieve these objectives:

- Synthesis and characterization of CHA using precipitation, sol-gel, and hydrothermal techniques.
- Comparative analysis of CHA synthesized by different methods.
- Development and characterization of composites of CHA with eugenol.
- Evaluation of the potential bio-applications of hydroxyapatite-eugenol composite.

1. LITERATURE REVIEW

1.1 Calcium hydroxyapatite

Calcium hydroxyapatite [CHA; $Ca_{10}(PO_4)_6(OH)_2$] is a calcium phosphate-based bio-ceramic material that has been the interest of researchers working in different areas of specialties, such as orthopedics, maxillofacial surgery, and biomedical fields [16] because of its chemical composition which is similar to that of human bone and teeth [17-20], and its high biocompatibility [21-23]. Moreover, it is a bioactive material that can provide cell proliferation of different types of cells. CHA's distinctive features, including its osteoconductive properties and ability to boost tissue and bone regeneration, increase its potential for fulfilling its uses in interdisciplinary fields.

1.1.1 General features

It is always essential to consider the biomaterial's chemical, physical, structural, and biological properties before using it for biomedical applications. The composition, physical structure, and biological properties of CHA play critical roles in potential applications. It is a member of the apatite family, which contains calcium and phosphate in its composition, as well as fluorapatite and chlorapatite. The crystal structure of CHA is hexagonal; it consists of an array of PO_4 tetrahedra held together by Ca ions interspersed among them; its structure has OH ions (Fig. 1), which can be substituted by fluoride, chloride, or carbonate, resulting in fluorapatite, chlorapatite or carbonate apatite, respectively [24]. Other than that, replacing Ca^{2+} and PO_3^{4-} in CHA is still possible [25]. The substitution in its structure can significantly change its structural characteristics [26, 27] and physicochemical and biological properties [25].

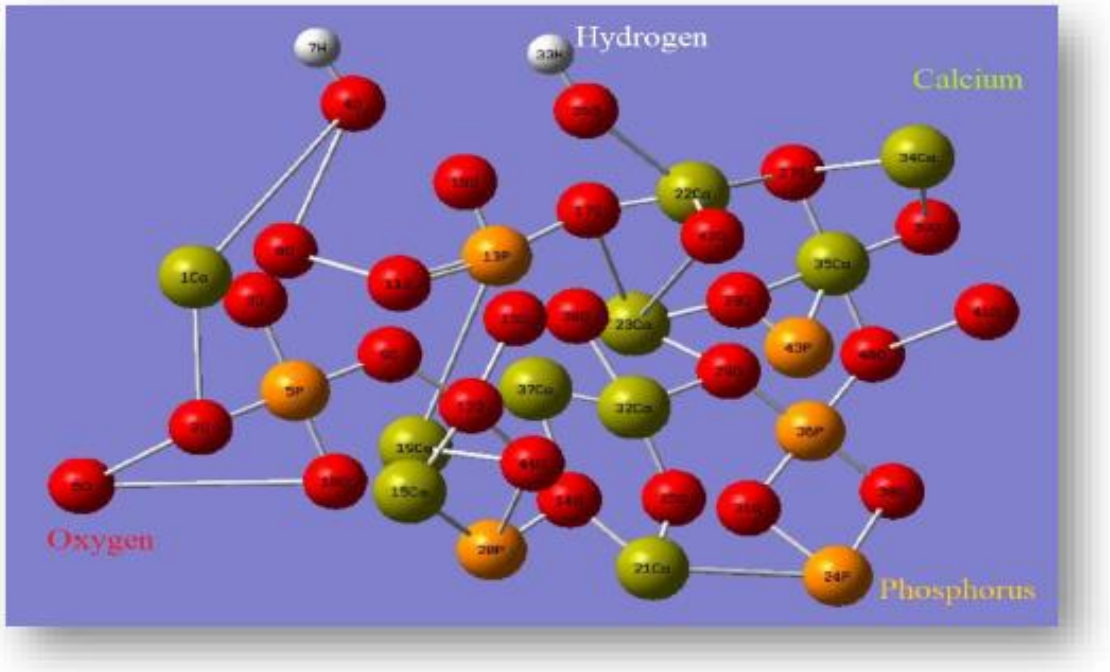

Fig 1. Crystal structure of hydroxyapatite [38]

CHA is a free-carbonate stoichiometric apatite phase with a calcium-to-phosphate Ca/P ratio 1.67 [28, 29]. CHA is the most stable thermochemically in various factors such as pH, temperature, and the content

of human biological conditions. CHA is moderately resorbable in physiological environments, which means it can gradually be replaced by natural bone [29]. Its bioactivity is one of its characteristics, raising its potential to induce tissue and bone regeneration. As for its mechanical properties, CHA is brittle, which limits its use in areas that require high load force [30]. It can be obtained from natural or synthetic sources [31]. Natural CHA can be prepared from eggshells [32-34], fish bones [35], coral [36], or bovine [37]. Although CHA can be found in nature as calcium apatite, it needs to be chemically synthesized to encounter specific properties, which include purity and morphology.

1.1.2 Synthesis methods

Researchers have utilized various methods for synthesizing calcium phosphate (CaP) biomaterials, namely calcium hydroxyapatite, as will be discussed in this section. CHA is formed in the Ca-PO_4-H_2O through a reaction of the starting materials; the reaction should contain Ca^{2+} and PO_4^{3-} ions, and a combination of these sources could be used to prepare CHA using a specific method. The selection of both ionic sources usually involves salts to avoid the formation of other CaP phases. For instance, using phosphoric acid (H_3PO_4) as the phosphate source could form the precipitation of the brushite phase [39]. Applying high temperatures during the synthesis can result in immensely high crystallinity, significantly different from natural bone [40]. On the other hand, biomaterials synthesized under low temperatures could exhibit low crystallinity and, thus, demonstrate more excellent tissue compatibility [41]. Synthesis methods, such as sol-gel [42], hydrothermal [43], and co-precipitation [44-46].

1.1.1.1 Sol-gel method

This method effectively synthesizes the nanostructured hydroxyapatite phase because it allows for strictly controlled process parameters [47]. Sol-gel uses a mixture of calcium and phosphate to obtain CHA to a significant extent. Some of the authors used organic materials in the sol-gel technique. Masuda et al. [48] demonstrated that the sol-gel could synthesize the CHA method by using calcium ethoxide [Ca $(OC_2H_5)_2$] and Triethyl phosphite [$P(OC_2H_5)_3$] as precursors of metal alkoxides. Then again, the alkoxide was altered instantly using calcium or phosphorus inorganic precursors. Li et al. [49] reported that applying the sol-gel process efficiently produces CHA with improved stability at biomaterial/host bone interfaces in vivo and in vitro experiments. However, calcium nitrate tetrahydrate [Ca $(NO_3)_2 \cdot 4H_2O$)] has been widely used and selected as a calcium precursor for the synthesis of CHA in combination with phosphate precursor in the sol-gel technique [50].

Although various precursors of calcium and phosphate can be used in this process, the chemical reactivity and the temperature for the formation of the apatite structure during the synthesis of CHA primarily depend on the chemical nature of the precursors. Balamurugan et al. [47] employed calcium nitrate tetrahydrate and triethyl phosphate as calcium and phosphate precursors, respectively, with a Ca/P ratio of 1.67, then the resulting CHA powder was thermally heated at a range of different temperatures up to 900°C. Brendel et al. [51] synthesized CHA using calcium nitrate tetrahydrate and phenyl-diclorophosphine [$C_6H_5Cl_2P$] as precursors at low temperatures (400°C). However, the obtained CHA resulted in low purity and poor crystallinity. Increasing the temperature to 900°C resulted in a pure and highly crystallized CHA phase.

On the other hand, many researchers suggest using phosphorous pentoxide [P_2O_5], calcium nitrate tetrahydrate, or calcium acetate monohydrate [$Ca(CH_3COO)_2 \cdot H_2O$)] as precursors for synthesizing CHA

powders [52]. They usually dissolve the raw materials in ethanol by stirring and/or refluxing them. Different solvents, such as 2-butanol, ethanol, and water, were used to prepare the solvents (see Fig. 2) [53]. However, the potential drawback is the formation of the β-tricalcium phosphate [β-TCP; $Ca_3(PO_4)_2$] phase in addition to CHA when the surfactant's concentration was not optimized [54].

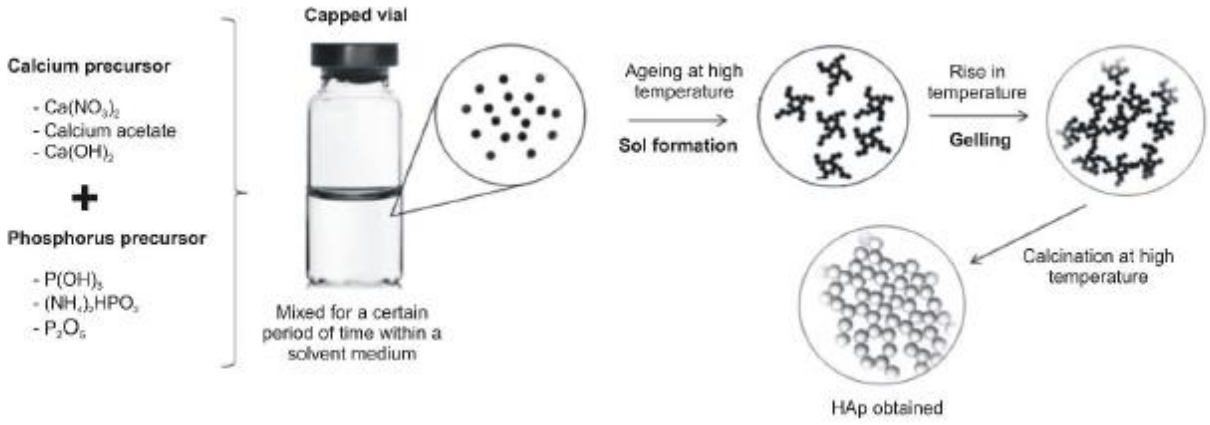

Fig 2. Sol-gel method for synthesis of CHA diagram [53]

1.1.1.2 Hydrothermal method

This method is one of the standard methods for producing CHA in an aqueous solution under pressure and high temperatures in an autoclave or hydrothermal vessel. Organic modifiers could be used to control the morphology and structure of crystals [55-57]. This procedure can obtain high-crystalline CHA powder.

The following reactions would produce CHAp:

$$4Ca(OH)_2 + 6CaHPO_4{\bullet}2H_2O \longrightarrow Ca_{10}(PO_4)_6(OH)_2 + 18H_2O \quad (1)$$

or

$$10CaCO_3 + 6(NH_4)_2HPO_4 \longrightarrow Ca_{10}(PO_4)_6(OH)_2 + 6NH_3{+}2H_2O + 10CO_2 \quad (2)$$

This technique's required pressure and temperature are favorable for increasing the reactivity and creating chemical bonds that ensure the formation of a stoichiometric and CHA with high crystallinity [56]. Additionally, Huang et al. [55] reported that the interactive effect of pressure and temperature produced high-crystalline CHA without any further post-treatment. Moreover, Zhang et al. [58] synthesized CHA with high purity by hydrothermal reaction between calcium chloride [$CaCl_2$] and phosphoric acid [H_3PO_4] at 100°C for 10 hours.

When calcium hydroxide [$Ca(OH)_2$] and ammonium phosphate [$(NH_4)_3PO_4$] were used in a hydrothermal method at 200°C for 24 h, CO_3 substituted CHA with a Ca/P ratio from 1.86 to 2.08 was

formed [59]. In contrast, Wang et al. [60] applied a hydrothermal reaction with low temperatures ranging from 60 to 150C for 12 to 24 h, using $CaCl_2$ and dipotassium hydrogen phosphate [K_2HPO_4], which resulted in CHA with pure crystalline phase. Also, Nagata et al. [61] employed the hydrothermal method using calcium nitrate tetrahydrate and diammonium phosphate [$(NH_4)_2HPO_4$]; the resulting material had pure and crystalline phases. However, there were inconsistencies in shapes and sizes. Therefore, several studies have used surfactants like cetyltrimethylammonium bromide (CTAB) [57,62], as well as a chelating agent like ethylene diamine tetra-acetic acid (EDTA) [63] to control the morphology of CHA. Manafi et al. [43] reported the successful synthesis of nanostructured CHA by dissolving calcium hydrogen phosphate dihydrate [$CaHPO_4{\cdot}2H_2O$] and sodium hydroxide [NaOH] in distilled water and then adding CTAB. The synthesis was regulated at 150°C for 2 hours.

In summary, hydrothermal can produce CHA with higher crystallinity. Moreover, this method results in controllable particle size and morphology of the obtained materials by adding modifiers such as EDTA and CTAB.

1.1.1.3 Precipitation reaction method

The precipitation method is one of the broadest techniques used by researchers for the synthesis of CHA. It uses an aqueous solution, known as wet, chemical, or aqueous precipitation. The reaction occurs between calcium and phosphorus ions, with controlled pH and temperatures [64]. The chemical precipitation method is the most researched technique for synthesizing CHA. In contrast to the other available methods, it was widely chosen for the synthesis of CHA since it presents a simple process and has a relatively low cost [44]; additionally, it produces CHA with characteristics similar to those of bone and dental tissues. The precipitation method goes through a series of procedures. Initially, reagents containing calcium and phosphate are mixed; for the Ca^{2+} source, the candidates are calcium hydroxide [$Ca(OH)_2$] or calcium nitrate [$Ca(NO_3)_2$]. For the PO_4^{3-} source, the candidates are orthophosphoric acid [H_3PO_4], or diammonium hydrogen phosphate [$(NH_4)_2HPO_4$]. Next, the mixture is adjusted to a specified pH, and the reaction is from room temperature to the boiling point of water [65,66]. Some studies have investigated the optimal pH to use during the synthesis of CHA. Based on Afshar et al. [67], the precipitated Ca^{2+} in the CHA decreases with pH reduction. The mixture is stirred to allow the crystal growth and the precipitation of CHAp. Finally, the obtained precipitate will be filtered, washed to remove any by-products, and dried before being ground into powder form [68].

Yagai and Aoki first stated this method, as Bouyer et al. [69] indicated calcium hydroxide [$Ca(OH)_2$] and phosphoric acid [H_3PO_4] were used as the starting materials in the following reaction;

$$10Ca(OH)_2 + 6H_3PO_4 \longrightarrow Ca_{10}(PO_4)_6(OH)_2 + 18H_2O \quad (3)$$

This reaction produced only water as a byproduct. The particle size, shape, and surface area of CHA were highly susceptible to the rate of phosphoric acid and the reaction temperature; in particular, the addition rate was firmly connected to the solution's pH. Temperature was a definitive factor in the crystal structure.

Moreover, for the synthesis of CHA, calcium nitrate or calcium chloride can be used as calcium sources with ammonium hydrogen phosphate at a pH higher than 4.2, adjusted with ammonium

hydroxide. The reaction temperature can vary between room temperature ~ 100°C [70, 71]. The reaction can be shown as follows (4):

$$10Ca(NO_3)_2 + 6(NH_4)_2HPO_4 + 8NH_4OH \longrightarrow Ca_{10}(PO_4)_6(OH)_2 + 20NH_4NO_3 + 6H_2O \quad (4)$$

Rigo et al. [72] used the precipitation method to produce CHA powder; clinical studies of this product demonstrated advanced bone tissue regeneration.

Moreover, Ghosh and Sarkar [73] conducted a study for synthesizing CHA using different methods (precipitation, sol-gel, and combustion). This study showed that CHA produced through precipitation had the highest density and hardness. Furthermore, its bioactivity was favorable compared to the other methods. Therefore, we can conclude that precipitation is the most suitable method to produce CHA with improved bioactivity. A schematic diagram of the synthesis of CHA by the chemical precipitation method is shown in Fig. 3.

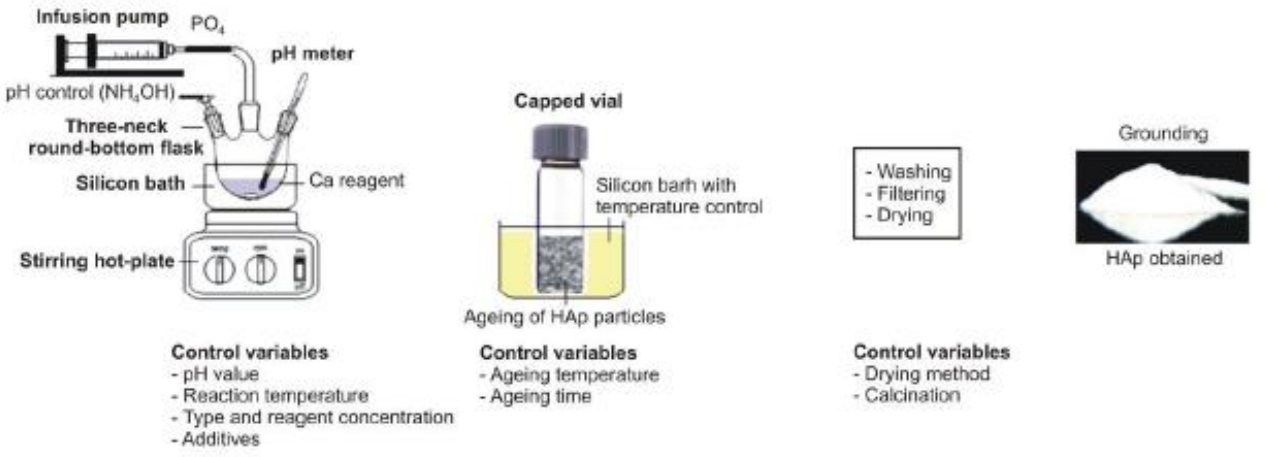

Fig 3. Chemical precipitation method for synthesis of hydroxyapatite diagram [53].

1.1.3 Application in Medicine

The first artificial biomaterial used in history was Plaster of Paris or Calcium sulfate [$CaSO_4$] [74, 75], but its drawbacks limit its clinical uses. In the period of (1876 – 1945) Fred Houdlette Albee invented bone grafting [76]. He first attempts to implant calcium phosphate [$CaPO_4$] as an artificial biomaterial to repair bone defects in rabbits [77]. Also, he invented other advances for their uses in orthopedic surgery [75]. At present, CHA has drawn much attention and interest as a biomaterial with much potential for applications in various fields related to medicine [78-80]. Among the applications, CHA can be used in drug delivery systems, implants, dentistry, bone grafting, and tissue engineering.

Drug carrier in the recent decade, CHA has been used as a drug carrier. For instance, nanoparticles have been applied to control the release of many proteins and drugs [81]. CHA is used to supply antibiotics to the hard tissue [82] and other medications as an anticancer substance [83-85], anti-

inflammatory [86-89], and some other molecules such as vitamins, hormones, and growth factors [90-92]. For drug release, differences in the morphology of CHA permit the loading of drug capacities, particularly CHA with microspheres with hollow structures, accelerating the loading of drugs and their controlled release [93]. In this context, Ibrahim et al. [94] synthesized CHA using eggshells at room temperature with a pore volume of (1.4 cm^3/g) and a surface area of (284.1 m^2/g); the obtained CHA with these characteristics developed the incorporation of ibuprofen, dissolution, and the controlled release of drug through carbon dioxide [CO_2].

Tissue engineering Bone grafts could be defined as a material that can replace and regenerate bone when implanted into the bone defect. They are necessary to treat bone lesions resulting from infections**,** tumors, or trauma. However, some drawbacks may originate from donor site compatibility and immune system rejection. Therefore, applying biocompatible scaffolds is an alternative for bone healing because they can ensure cell proliferation, differentiation, and tissue regeneration. An additional characteristic of the bone graft is its highly porous structure with interconnected pores, which allows cell migration to the defect site and promotes new bone tissue regeneration. Macropores in the scaffolds are favorable for allowing the formation and mineralization, hence, the migration of osteoblasts. Meanwhile, the micropores improve vascularization by blood supply and nutrient diffusion for bone reconstruction [95,96].

In Dentistry, the most distinctive characteristic of CHA for **maxillary sinus augmentation (MSA)** is its sponge-like structure compared with the other granular graft materials, as it can easily be compressed and placed in any desired site for MSA. Ohba S et al. [97] applied CHA to augment the maxillary sinus floor. He concluded from his study that there were no signs of infections. Furthermore, it enhances the development of mature bone because of its adequate pore size required for cell migration.

Dental implants are a successful treatment option for replacing teeth. However, a bone defect may sometimes be significantly large, making replacing the defect with an implant challenging. Therefore, bone reconstruction using a bone graft is required before placing the dental implant.

Periodontal bone defects and alveolar bone destruction are outcomes of chronic periodontal disease; this results in infra-body defects that need long-term care. The reconstruction of these bony defects is ordinarily done through guided tissue. Regeneration using barrier membrane and guide bone regeneration (GBR) using CHA as graft material is a successful option for treatment [98]. Kamboj et al. [99, 100] evaluated the efficacy of CHA in treating bony defects and concluded that it showed a significant reduction in the depth of the dental pocket.

1.2 Composites of calcium hydroxyapatite

The evolution of biomaterials has continued over the years as new methods and innovative materials have been investigated and developed due to their high demand in numerous biomedical applications. The progression of materials for biomedical applications started from bioinert materials such as stainless steel, zirconia, etc., which are biocompatible but inactive [101-103]. On the other hand, bioactive materials can interact with tissue and surroundings [104]. Biodegradable and bioactive materials have been utilized for bone tissue regeneration because of their superior cell adhesion, differentiation, and proliferation [105]. Moreover, bioactive materials can construct an organic bond with the surrounding

tissues and release antibacterial/antioxidant agents [106]. CHA is an example of bioactive materials and biopolymers [107].

Polymer-based composites, including polyethylene (PE) and high-density polyethylene (HDPE), are combined with CHA to improve their biological properties, and they are used in implants for orthopedic applications. Liu et al. [108] introduced HDPE/CHA composites with excellent mechanical performance and good biocompatibility in vivo. Poly (lactic-co-glycolic acid) (PLGA) is another polymer material that can be used with CHAp. Park et al. [109] prepared PLGA/CHA composite using the melt reaction method, with high efficacy as bone grafting material (see Fig. 4). There are many other polymers to be used, such as polyesters like poly (lactic acid) (PLA), poly-caprolactone (PCL), and poly(L-lactic acid) (PLLA) [110-115], and their composites have attracted interest due to their outstanding biodegradability and biocompatibility. These polymers are not toxic to the body, as they can gradually degrade within the body, leaving no residue and no side effects on the tissues. However, they have some drawbacks that limit their use; polyester materials have lower mechanical strength when compared to metals. To overcome these limitations, adding a bio-ceramic material into polyesters could considerably enhance its bioactivity and regulate the acidic degradation environment, eliciting new bone formation and hindering inflammatory reactions [116].

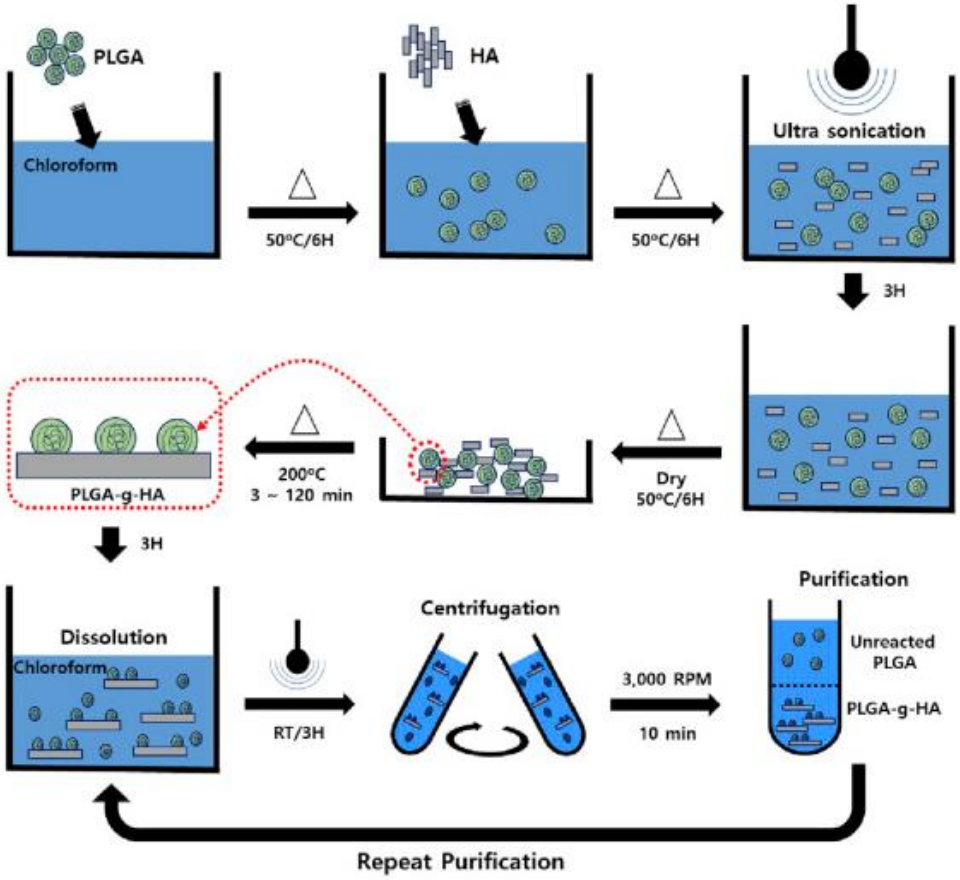

Fig 4. Process of preparing PLGA-g-CHA composites [109]

Ceramics-based composites: Matsumoto et al. [117] investigated a CHA incorporated with zirconia (ZrO_2) with a microporous structure, and the results revealed that the obtained composites had strength in the range of cortical bone strength—also, Bulut et al. [118] studied the biocompatibility of CHA/zirconia and alumina composites as well, the results showed excellent mechanical properties of the CHA/ZrO_2 composites along with development of bioactive properties. Moreover, Chopra et al. [119] fabricated a composite of zinc-doped CHA nanorods using a one-pot hydrothermal technique. The obtained composites demonstrated improved protein adsorption and potential for osteoconductive and osteoinductive properties. Moreover, it promoted accelerating bone regeneration and vascularization in a rat model.

Some drawbacks of zirconia and alumina may arise, such as poor bioresorbability, brittleness, and high stiffness, leading to stress shielding and limiting their uses.

Metal-based composites have long been employed as a coating material on titanium (Ti) implants and have exhibited great results [120]. Porter et al. [121] revealed that CHA coating with Ti accelerated the implants' healing compared to the uncoated implants. Thus, CHA implants coated with Ti promoted bioactivity. However, they could produce poor bonding between CHA and Ti surfaces, leading to flaking of the implant.

1.3 Eugenol

Eugenol (EUG) (Fig. 5) is eco-friendly, inexpensive, and abundantly present.

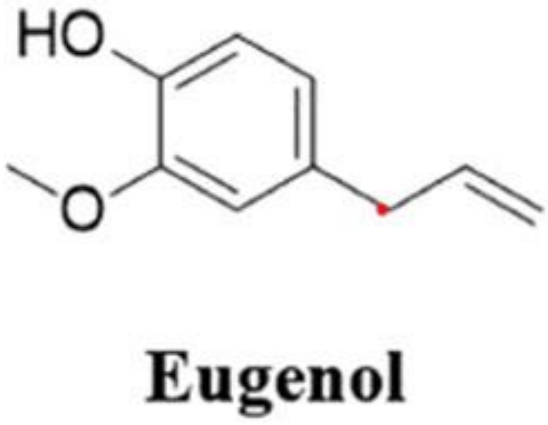

Fig 5. Structure of eugenol [129]

It is a widely known and well-investigated compound, a clove essential oil phenolic component. It is mainly an extracted component with about 70-90% clove oil and is responsible for the clove aroma. It was first isolated from Eugenia caryophyllata buds and leaves and introduced as a volatile compound in 1929. It was commercially produced in 1940 in the United States of America (USA) [122-126]. EUG is extracted from natural ingredients like nutmeg oil, cinnamon, and many other plants [122,127]. EUG was used in ancient Chinese medicine. Currently, it has a wide range of therapeutic and practical applications. When evaluated against fungi, *Cladosporium spp*. and EUG exhibited favorable antioxidant

and antimicrobial properties [128,129]. It also showed antimicrobial effects against several human pathogens, including broad Gram-negative and Gram-positive bacteria, fungi types, and several species [130]. Some publications reported other activities, such as antiviral and anti-inflammatory [131]. In addition, reports showed antibacterial activity, which can work through interactions with the cell membrane of bacteria [132].

1.3.1 Chemical properties

Eugenol (4-allyl-2-methoxyphenol) with the chemical formula [$C_{10}H_{12}O_2$] is a phenylpropanoid, a colorless to pale-yellow oil with a strong spicy aroma, and pungent odor of clove and tangy taste, with a molecular weight of 164.2 g/mol. This molecule is considered a weak acid, moderately soluble in water but well soluble in organic solvents, such as ethanol, methanol, etc. [122,129].

EUG has low chemical solubility and is sensitive to oxidation and numerous chemical interactions; when taken orally, it is rapidly absorbed via the small intestines and metabolized in the liver [126,129]. Based on its chemical structure, eugenol has a benzene ring and allyl, methoxy, and hydroxyl functional groups; this will make it possible to obtain other beneficial derivatives of eugenol [133,134].

EUG reacts with many strong alkalis. For example, when exposed to air, EUG's texture becomes thicker, and its color turns darker. It also gets blackened with time and may decay when exposed to light [135].

1.3.2 Application in Dentistry

Presently, dental materials are not required to be exclusively biocompatible but also to have an antibacterial effect [136,137]. In dentistry, EUG is acknowledged for its analgesic and anesthetic properties [138]. It has been applied in combination with Zinc Oxide (ZOE) as a coating material for pulpotomy procedures on primary teeth, where the infected part of the coronal pulp tissue is removed, followed by the placement of the combination of ZO and EUG. Aside from this use, it can be found in oral care products, as it has been shown to hinder teeth's decalcification caused by taking acidic drinks and promoting remineralization [139-141].

EUG plays a significant role in the dental field. It is also a sensitizer and can produce local anesthesia. Furthermore, EUG-producing dental materials are used in clinical dentistry. ZOE is applied to the dental cavity; small amounts of eugenol disperse through the dentine to the pulp in lower concentrations; as pointed out earlier, it has anti-inflammatory and local anesthetic effects on the dental pulp. Thus, using ZOE as a temporary dental filling may promote pulpal healing. ZOE is also used as an endodontic sealer to impact the healing of the periapical tissue. Moreover, eugenol is a popular painkiller due to its ability to inhibit voltage-gated sodium channels (VGSC) in the primary supply neurons of the teeth [142]. Hwang et al. [143] investigated the effect of EUG using a rat model; his study demonstrated that a combination of EUG and capsaicin can be a pain-selective local analgesic in the orofacial region. It demonstrates anti-nociceptive activity; it is also used with prilocaine/ lidocaine in topical applications to reduce pain [144].

In addition, post-to-root canal treatment, coronal leakage is considered a significant reason for endodontic treatment failure [145]. In vitro studies have demonstrated that the rapid penetration of bacteria in the root canal system will increase without a coronal seal over the root filling [146,147]. Therefore, applying a base to root canal filling has decreased microleakage and expanded the long-term prognosis of root canal-treated teeth [148,149]. ZOE restorative material is also used as a base beneath

the permanent filling between visits to prevent bacteria from accessing the root canal. It is thought that the free hydroxyl groups in eugenol can cause damage to the cell membrane by altering the membrane permeability, giving the ZOE-based materials their antibacterial and bacteriostatic effects [150,151]. Niyaz Ahmed et al. [152] investigated the impact of using eugenol-Nano emulsion-Carbopol gel (EUG-NE-Gel), significantly reducing the alveolar bone and treating periodontal diseases.

Although eugenol has multiple properties and is commonly used in the dental field, it was reported to have side effects such as irritation and allergy for dentists and burning mouth syndrome [153]. Opdyke et al. [154] stated that eugenol (≤ 5%) is safe for topical application. Considering the various benefits and advantageous features of CHAp and EUG, our study aimed to investigate the development of CHAp/EUG composites and evaluate their potential for antibacterial activity.

2. EXPERIMENTAL

This section details the methodologies employed for synthesizing and characterizing calcium hydroxyapatite [CHA; $Ca_{10}(PO_4)_6(OH)_2$] and its composite with eugenol. The synthesis procedures were designed to compare different methods for CHA preparation, while the characterization techniques were used to assess the synthesized materials' structural, morphological, and antibacterial properties.

2.1 Synthesis

CHA was synthesized using three different methods:

1- Sol-gel
2- Hydrothermal
3- Precipitation techniques

These methods were selected to evaluate their effects on particle morphology, crystallinity, and bioactive properties. During synthesis, CHA with eugenol composites was prepared by incorporating eugenol into its matrix.

2.1.1 Sol-Gel Method

Reagents used

1- Calcium acetate monohydrate ($Ca(CH_3COO)_2 \cdot H_2O$, ≥99%, Carl Roth)
2- Diammonium hydrogen phosphate ($(NH_4)_2HPO_4$, ≥97%, Carl Roth)
3- Polyethylene glycol (PEG 1500, M_n 1400-1600 g/mol, Carl Roth)
4- Ammonia aqueous solution (NH_3, ≥25%, Carl Roth)
5- Distilled water

The sol-gel method synthesized CHA, utilizing calcium acetate hydrate as the calcium source and diammonium hydrogen phosphate as the phosphate source. This process involved solution preparation, polymer incorporation, pH adjustment, gel formation, and subsequent calcination to obtain the final powder.

Solution Preparation

Two 200 mL beakers were each filled with 25 mL of distilled water. In one beaker, 2.377 g of $(NH_4)_2HPO_4$ was dissolved, while in the other beaker, 5.285 g of $Ca(CH_3COO)_2 \cdot H_2O$ was added. Both solutions were stirred continuously using individual magnetic stirring bars, and the beakers were covered with Petri dishes to prevent evaporation.

Preparation of PEG Solution

A 6% PEG solution was prepared separately by dissolving 6 g of PEG in 94 mL of distilled water under constant stirring. Once fully dissolved, 25 mL of the solution was added to each beaker containing the calcium and phosphate solutions. The temperature was maintained at 55 to 60°C while stirring for 30 minutes to ensure thorough mixing.

pH Adjustment

To initiate the sol-gel process, 20 mL of NH_3 was gradually added to both beakers while monitoring the pH until it reached 11. The temperature was then increased to 65–80°C, and the solutions were stirred for an additional 20 minutes to promote homogeneity. The two solutions were combined into a covered beaker and stirred for another 30 minutes to prevent excessive evaporation.

Gel Formation and Drying

The combined suspension was subjected to controlled evaporation at 80–100°C, which formed a Ca-P-O gel. This gel was dried at 150°C for 24 hours to remove residual moisture and enhance the material's structural integrity.

Calcination

The dried gel was calcinated at 400, 600, 680, and 800°C for 5 hours to promote phase transformation and crystallization. The temperature increased at a controlled heating rate of 1°C/min from room temperature. Between each calcination step, intermediate grinding was performed using an agate mortar and pestle to ensure the uniformity of the final product.

The resulting powder was further analyzed using scanning electron microscopy (SEM), X-ray diffraction (XRD), and Fourier-transform infrared spectroscopy (FTIR) to evaluate its structural and morphological characteristics.

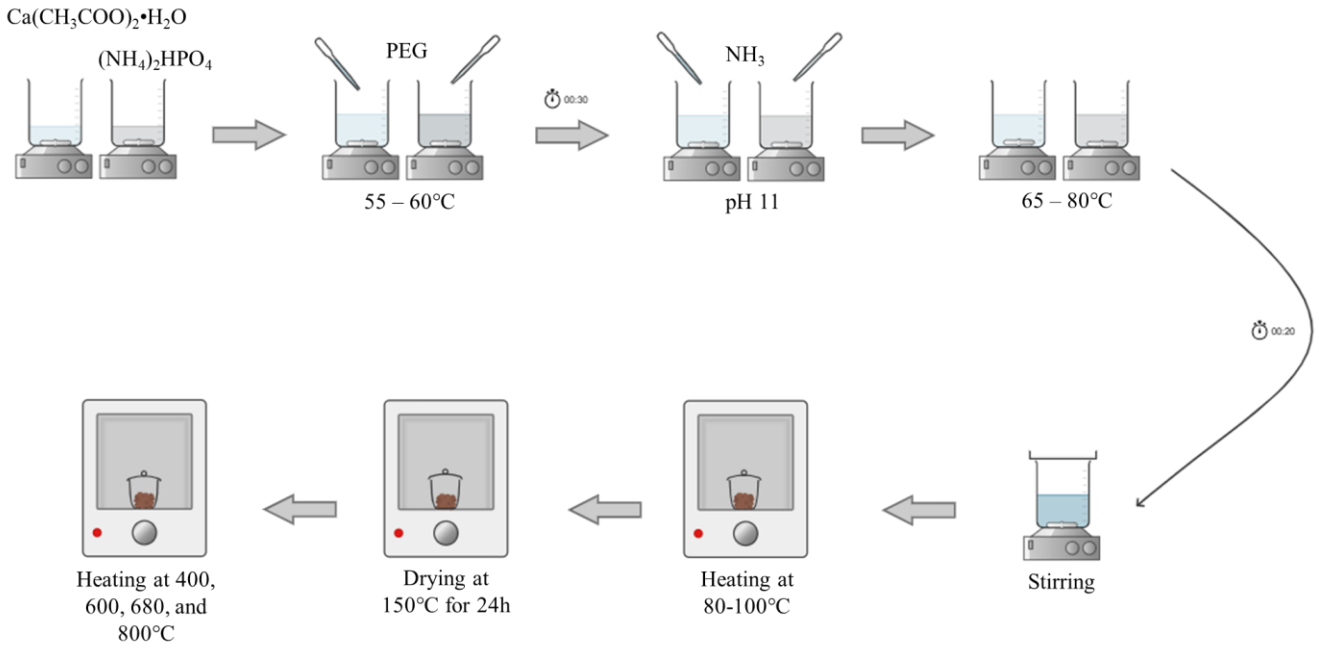

Fig 6. The schematic diagram for the synthesis of CHA by sol-gel method.

2.1.2 Hydrothermal Method

Reagents Used

1- Calcium nitrate tetrahydrate $Ca(NO_3)_2 \cdot 4H_2O$, ≥99%, Carl Roth)
2- Diammonium hydrogen phosphate ($(NH_4)_2HPO_4$, ≥97%, Carl Roth)
3- Ammonia aqueous solution (NH_3, ≥25%, Carl Roth)
4- Distilled water
5- Acetone

The hydrothermal method was utilized to synthesize α-tricalcium phosphate (α-TCP: α-$Ca_3(PO_4)_2$) through a wet precipitation process, followed by hydrothermal treatment to achieve the desired phase

composition. The synthesis involved the preparation of precursor solutions, precipitation, filtration, freeze-drying, and final hydrothermal processing.

α-TCP synthesis by wet precipitation

6.84 g of $Ca(NO_3)_2 \cdot 4H_2O$ was dissolved in 40 mL of distilled water to prepare the precursor solutions. In comparison, 2.54 g of $(NH_4)_2HPO_4$ was dissolved in 30 mL of distilled water. To adjust the pH, 10 mL of 25% ammonia solution was added to the phosphate solution, adjusting the pH to 10. The solution was stirred for one minute, after which the calcium nitrate solution was rapidly added while stirring at 400 rpm. This resulted in a white precipitate, which was stirred continuously for 10 minutes to ensure homogeneity.

Filtration and storage

The precipitate was collected by Buchner funnel filtration apparatus under vacuum and washed thoroughly with 200 mL of deionized water to remove residual ions. The purified precipitate was then transferred to a container and refrigerated for 15 minutes before freeze-drying.

Freeze-drying (Lyophilization)

The freeze-drying process was carried out to remove moisture from the precipitate without affecting its structure. The lyophilizer was set up by turning on both control buttons, ensuring the rotatable knob was fixed in place. The system was allowed to warm up for 15 minutes before loading the samples. The refrigerated precipitate was covered with tissue paper, secured by a rubber band, and placed on the lyophilizer plate. A glass dome cover was used to seal the setup, and the freeze-drying process was initiated. The samples were lyophilized for 24–48 hours. Once complete, the samples were carefully removed by following the appropriate procedure: selecting the "Stand up" mode, waiting one minute, rotating the knob, pulling the dome, and extracting the dried samples. The equipment was cleaned and turned off after completion.

Final Processing

The freeze-dried powder was ground using an agate mortar and pestle to achieve uniform particle size. The final product was characterized using X-ray diffraction (XRD) to determine its phase composition before hydrothermal processing.

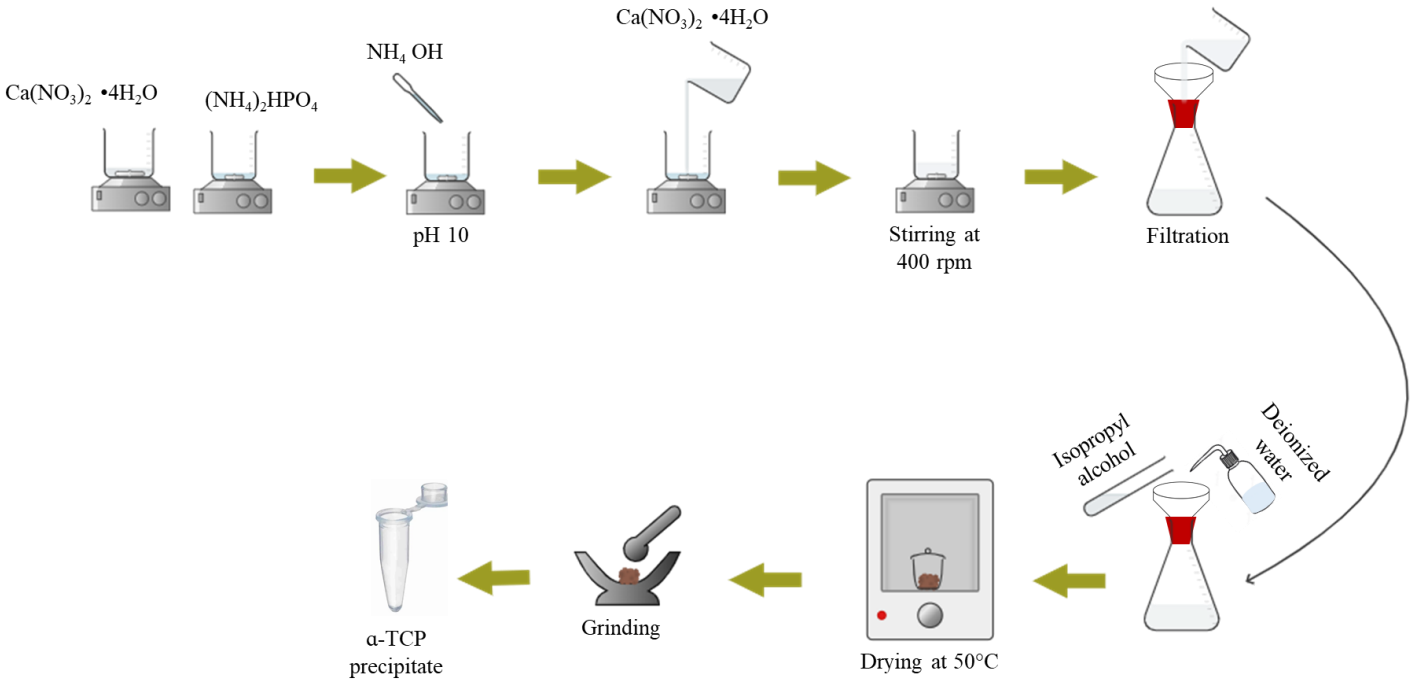

Fig 7. The schematic diagram for the preparation of α-TCP.

Hydrothermal Processing of α-TCP

Preparation

For hydrothermal treatment, 0.3 g of the synthesized α-TCP powder was weighed and transferred into a 90 mL PTFE-lined autoclave. To facilitate the hydrothermal reaction, 5 mL of distilled water was added.

Hydrothermal Treatment

The sealed autoclave was heated at 150°C for 3 hours to promote phase transformation and crystallization. After cooling, the treated sample was filtered and washed thoroughly with acetone to remove residual reactants. The washed sample was then dried at 50°C for 3 hours to eliminate moisture and obtain the final hydrothermally processed material.

The resulting product was further analyzed using XRD, FTIR, and SEM to evaluate its phase composition, structural characteristics, and morphology.

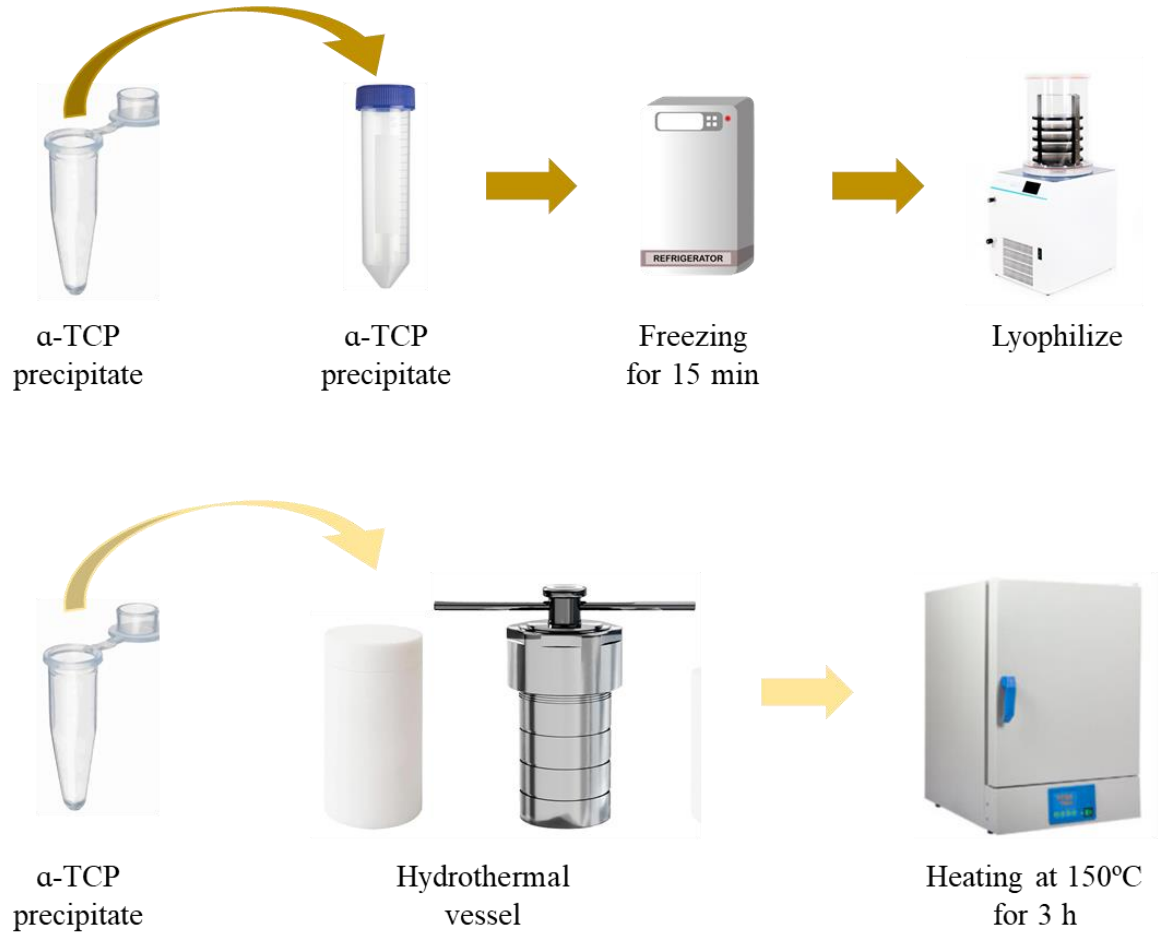

Fig 8. The schematic diagram for the synthesis of CDHA by the hydrothermal method.

2.1.3 Precipitation Method

Reagents Used

1- Calcium nitrate tetrahydrate ($Ca(NO_3)_2 \cdot 4H_2O$, ≥99%, Carl Roth)
2- Diammonium hydrogen phosphate ($(NH_4)_2HPO_4$, ≥97%, Carl Roth)
3- Ammonia aqueous solution (NH_3, ≥25%, Carl Roth)
4- Distilled water

The calcium and phosphate precursor solutions were prepared separately. Specifically, 3.1703 g of $Ca(NO_3)_2 \cdot 4H_2O$ was dissolved in 45 mL of distilled water, while 1.0564 g of $(NH_4)_2HPO_4$ was dissolved in 20 mL of distilled water. Both solutions were stirred until completely dissolved.

The precipitation reaction was initiated by gradually adding 8 mL of 25% ammonia to the $Ca(NO_3)_2 \cdot 4H_2O$ solution under continuous stirring. This was followed by rapidly adding the $(NH_4)_2HPO_4$

solution while maintaining a stirring speed of 750 rpm. The pH was adjusted to 10–11 and verified using litmus paper. The reaction mixture was stirred for 10 minutes, allowing the precipitate to form.

Afterward, the precipitate was collected using vacuum filtration with a Büchner funnel filtration apparatus and washed with 60 mL of distilled water. The filtered solid was then dried at 120°C for 12 hours at a heating rate of 1°C/min. The dried precipitate was ground using an agate mortar to obtain a fine powder, which was subsequently calcined at 800°C for 5 hours at a controlled heating rate of 1°C/min. Following calcination, the resulting powders from both methods were further analyzed using XRD, FTIR, and SEM to evaluate their structural and morphological characteristics.

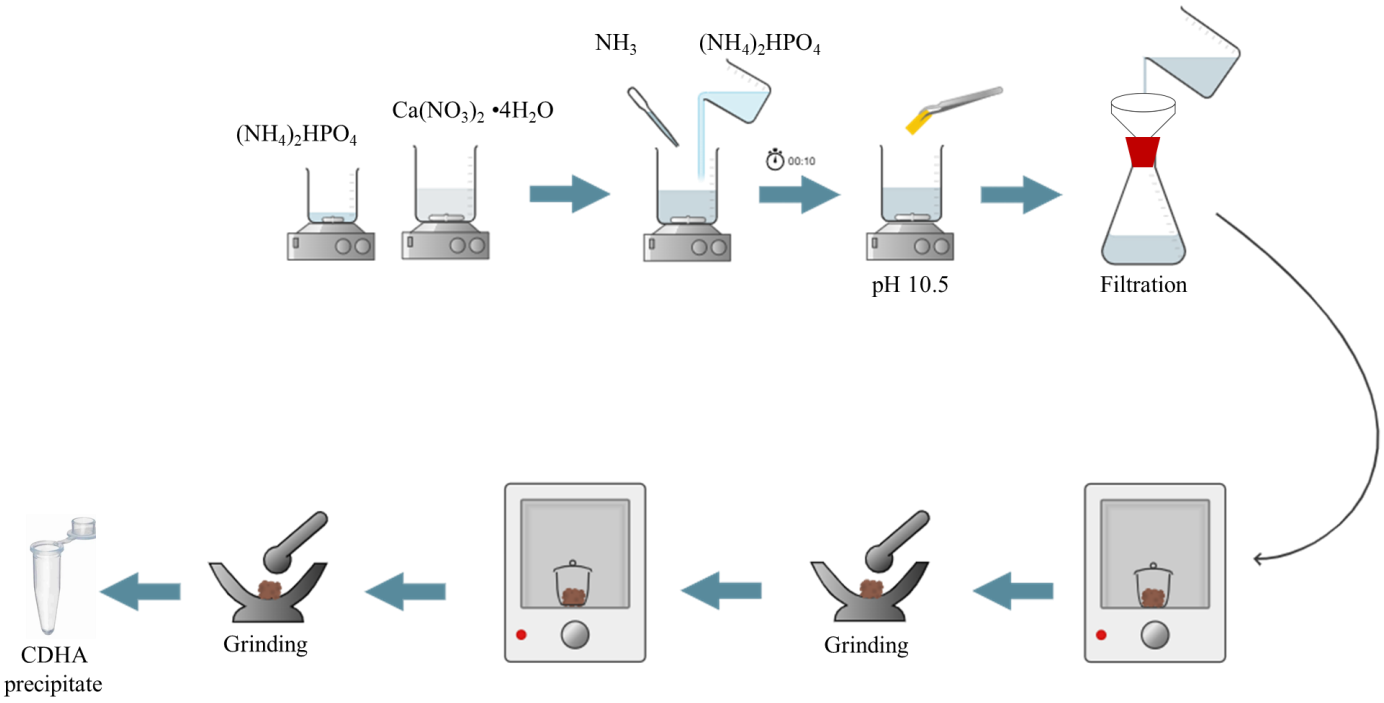

Fig 9. The schematic diagram for the synthesis of CHA by the precipitation method

2.2 Characterization

Various characterization techniques were employed to assess the structural, morphological, and chemical properties of the synthesized calcium hydroxyapatite (CHA) and its composite with eugenol. These include X-ray diffraction (XRD), scanning electron microscopy (SEM), Fourier-transform infrared spectroscopy (FTIR), and antibacterial testing. Each technique provided valuable insights into the material's composition, crystallinity, surface morphology, functional groups, and potential for biomedical applications.

Thermogravimetric Analysis (TGA)

The thermal decomposition of the materials was conducted using thermogravimetric (TG) analysis, using PerkinElmer STA 6000 for this purpose. 5-10 mg of material was heated from 25ºC to 900ºC at a 10ºC/min heating rate in a nitrogen atmosphere (20 mL/min).

X-ray Diffraction (XRD)

Powder X-ray diffraction (XRD; Rigaku MiniFlex II diffractometer) was analyzed to investigate the synthesized CHA's phase composition. The scanning was performed within the range of 10-60º 2θ at a scanning speed of 10 °/min

Fourier-Transform Infrared Spectroscopy (FTIR)

Fourier-transform infrared spectroscopy (FTIR; Bruker ALPHA spectrometer) was used to identify the functional groups in the synthesized CHA and CHA/eugenol composites. The FTIR spectra were recorded in the 400–4000 cm^{-1} range with a 4 cm^{-1} resolution.

Scanning Electron Microscopy (SEM)

The surface morphologies of the materials were observed using scanning electron microscopy (SEM; Hitachi SU-70 microscope, a Schottky-type field emission electron source)

3. RESULTS AND DISCUSSION

3.1 Comparative Study of Synthesis Methods for Calcium Hydroxyapatite

Calcium hydroxyapatite ($Ca_{10}(PO_4)_6(OH)_2$) was synthesized using three different techniques: sol-gel, hydrothermal, and precipitation. Each method successfully produced hydroxyapatite, but notable differences were observed in morphological structure, crystallinity, and thermal stability.

Physicochemical properties of the synthesized CHA

Fig. 10 demonstrates the results of the XRD of CHA synthesized by different methods. All samples showed XRD patterns typical of CHA, which confirms that all three approaches yielded single-phase CHA. The diffraction peaks matched well with the reference standard [PDF: 96-721-7895], and the strongest peak appeared near 2θ = 32°. It should be noted that the sol-gel-derived material showed particularly sharp and intense peaks, indicating a greater degree of crystallinity. This improvement in crystallinity is likely due to the higher temperatures applied during sol-gel synthesis, which promote better crystal growth and phase purity [156,157].

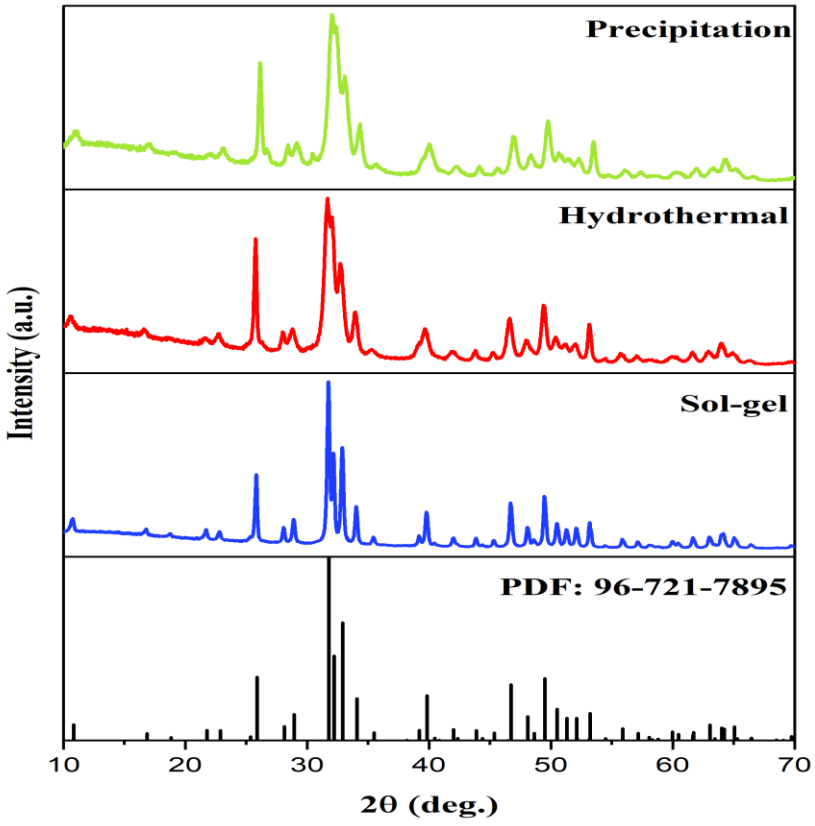

Fig 10. XRD patterns of CHA samples synthesized by sol-gel, hydrothermal, and precipitation methods. Vertical lines represent the standard XRD pattern of CHA [PDF: 96-721-7895].

The functional groups in the CHA samples were confirmed using FTIR, as shown in Fig. 11. The analysis of samples obtained by different methods demonstrated the presence of weak absorption bands at 3571 cm^{-1} and 633 cm^{-1}, which are assigned to the stretching vibration and the bending modes of the hydroxyl group, respectively. The characteristic bands for the phosphate group were detected at 1020-1090 cm^{-1}, 960 cm^{-1}, 560-600 cm^{-1}, and 430-470 cm^{-1}. A broad absorption band detected at 870 cm^{-1} was assigned to the P–O(H) stretching vibration of the hydrogen phosphate group, suggesting the formation of the calcium deficiency in the synthesized apatite-type material [158]. The bands observed at 1020-1090 cm^{-1} and 960 cm^{-1} were assigned to the phosphate group's asymmetric and symmetric P–O stretching vibrations, respectively. The bands detected in the 560-600 cm^{-1} spectral region are attributed to asymmetric O–P–O bending vibrations, whereas the 430-470 cm^{-1} region corresponds to symmetric O–P–O bending vibrations.

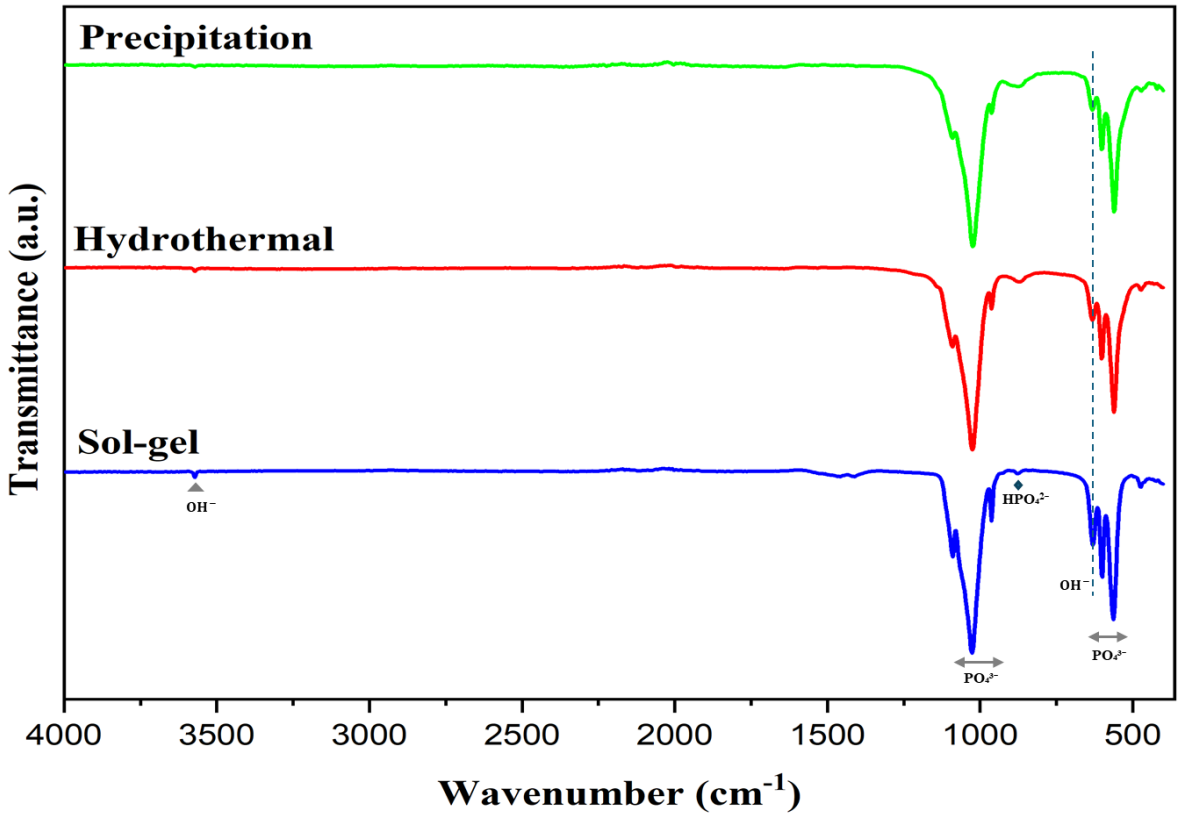

Fig 11. FTIR spectra of CHA samples synthesized by sol-gel, hydrothermal, and precipitation methods.

SEM examined the surface morphologies of the synthesized CHA samples. Fig. 12 illustrates the different morphologies of CHA acquired through sol-gel, hydrothermal, and precipitation reactions. The SEM images of the sol-gel-synthesized CHA in Fig. 12 (a) reveal relatively uniform particles, primarily resembling spherical-like crystals. Moderate agglomeration is noted, and the sample's surface is smooth, reflecting the influence of the relatively higher temperature required for the sol-gel method. Fig. 12 (b)

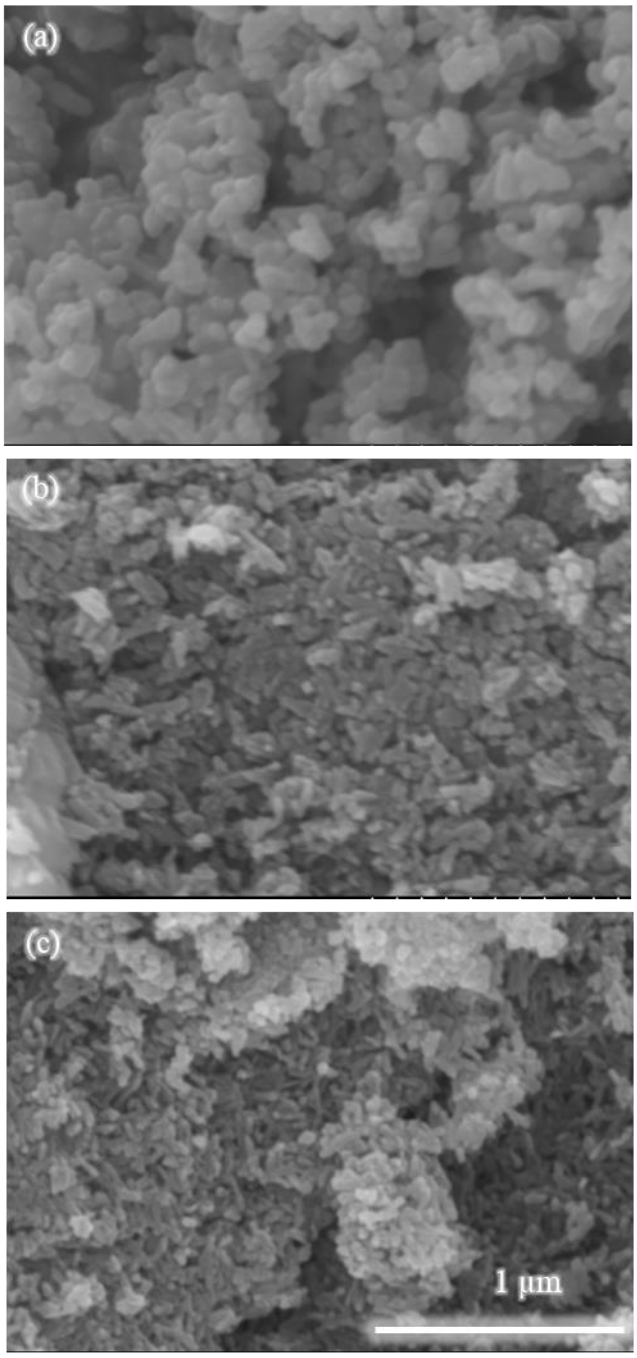

Fig 12. SEM images of CHA samples synthesized by sol-gel, hydrothermal, and precipitation methods.

show the CHA synthesized by the hydrothermal method, where particles display elongated rod-like crystals. The surfaces are smooth, and the crystals are well-defined, with minimal agglomeration present, indicating directional crystal growth under controlled conditions. Regarding the precipitation method, the surface of the samples depicted in Fig. 12 (c) shows particles with irregular shapes. Significant particle agglomeration is observed, accompanied by surface roughness.

In conclusion, based on the SEM images, the surface morphology of the produced CHA samples depended on the synthesis method.

TGA assessed the thermal stability of the synthesized CHA samples, as shown in Fig. 13, which revealed two main stages of weight loss.

This first stage occurred at a heating temperature ranging from 30 °C to approximately 300 °C. This weight loss is attributed to water and moisture loss from the samples. This phenomenon was observed in all samples regardless of the synthesis method. Furthermore, the samples produced by sol-gel demonstrated higher stability than the others, as they had the least weight loss. Further details of the weight loss are summarized in Table 1.

The second stage occurs between 600 °C and 800 °C, corresponding to the compounds' decomposition in the materials. Thermal degradations in the samples synthesized by hydrothermal and precipitation methods were significantly higher than those synthesized by the sol-gel process. This indicates the higher crystallinity of the latter samples.

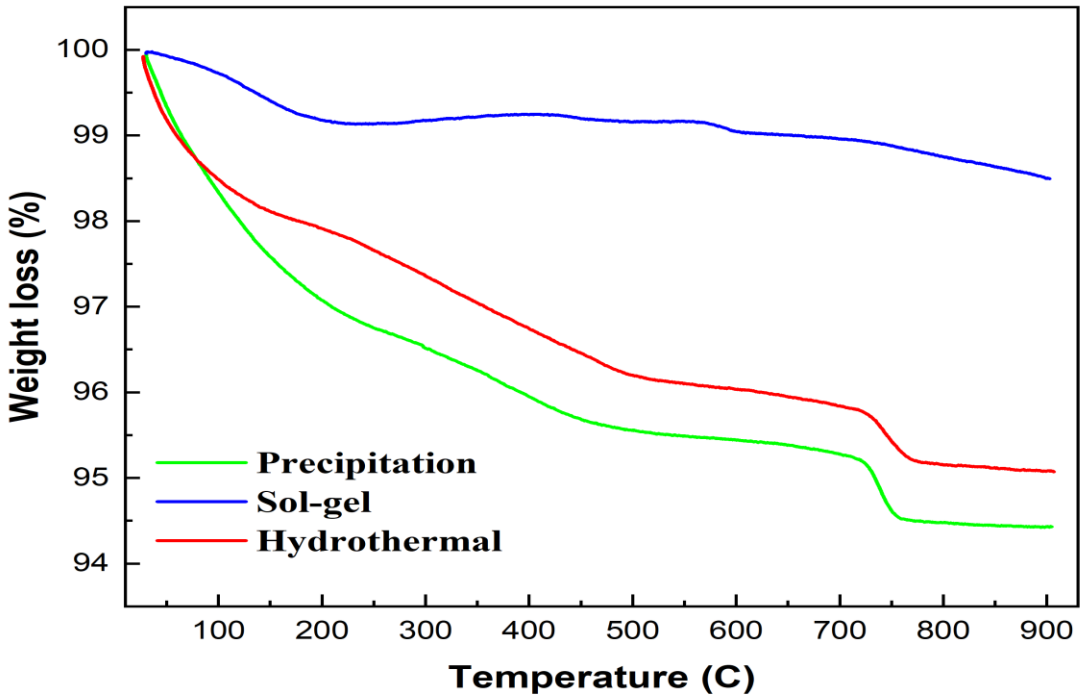

Fig 13. TG curves of CHA samples synthesized by sol-gel, hydrothermal, and precipitation methods.

Table 1. Weight loss of CHA samples synthesized by sol-gel, hydrothermal, and precipitation methods.

Synthesis Method	Weight Loss (30–300 °C) (%)	Weight Loss (600–800 °C) (%)
Sol-Gel	0.8%	0.3%
Hydrothermal	2.4%	0.9%
Precipitation	3.4%	1%

Conclusion

In the comparative study of synthesizing CHA using different methods, we concluded that the sol-gel synthesis produced CHA with the highest crystallinity, uniform particle structure, and higher thermal stability compared to other syntheses, which can be related to the higher temperature. The hydrothermal method generated crystals with clear morphology but moderate stability, whereas the precipitation method, though simple and scalable, resulted in materials with more structural imperfections and lower thermal resistance. These findings underline the sol-gel method as the most effective route for preparing high-quality calcium hydroxyapatite intended for advanced material applications. However, the higher crystallinity of the material might limit its use, since it can affect the resorbability of the material when implanted in the human body. Therefore, the precipitation method is considered for the synthesis method to produce CHA with lower crystallinity.

3.2 Formation of calcium hydroxyapatite composites with eugenol

Eugenol was introduced into the CHA synthesis using a precipitation method with distilled water to obtain HA-eugenol composites. Two concentrations of **eugenol (2 wt.% and 5 wt.%)** were prepared and added during the reaction before filtration.

Reagents Used

1- Calcium nitrate tetrahydrate ($Ca(NO_3)_2 \cdot 4H_2O$, ≥99%, Carl Roth)
2- Diammonium hydrogen phosphate ($(NH_4)_2HPO_4$, ≥97%, Carl Roth)
3- Ammonia aqueous solution (NH_3, ≥25%, Carl Roth)
4- Eugenol ($C_{10}H_{12}O_2$, >99%, Thermo Scientific)
5- Distilled water

Preparation of Eugenol Solutions:

- **2% Eugenol Solution:** 2 mL of eugenol was mixed with 98 mL of distilled water.
- **5% Eugenol Solution:** 5 mL of eugenol was mixed with 95 mL of distilled water.

Synthesis of CHA-Eugenol Composites:

The synthesis followed the previously described **precipitation method** using aqueous solutions of $Ca(NO_3)_2 \cdot 4H_2O$ and $(NH_4)_2HPO_4$ under alkaline conditions. The key steps were:

1. **Solution Preparation:**
    - 3.1703 g of $Ca(NO_3)_2 \cdot 4H_2O$ was dissolved in 45 mL of distilled water.

- 1.0564 g of $(NH_4)_2HPO_4$ was dissolved in 20 mL of distilled water.

2. **Mixing & pH Adjustment:**
   - 8 mL of 25% ammonia solution was added to the calcium solution under stirring.
   - The phosphate solution was added quickly under continuous stirring at 750 rpm.
   - The pH was adjusted to 10–11.
3. **Incorporation of Eugenol:**
   - Before filtration, 2% or 5% eugenol solution was added to the reaction mixture and stirred for 10 minutes at 270 rpm to ensure incorporation.
4. **Filtration & Drying:**
   - The precipitate was filtered using a Büchner funnel and a vacuum flask.
   - Washed with 60 mL of distilled water.
   - The final product was dried at 120°C for 12 hours.

🔷 **Note:** The **calcination step (800°C for 5 hours) was skipped** to retain the CHA composite's organic and bioactive eugenol compounds.

3.2.1 Synthesis and Characterization

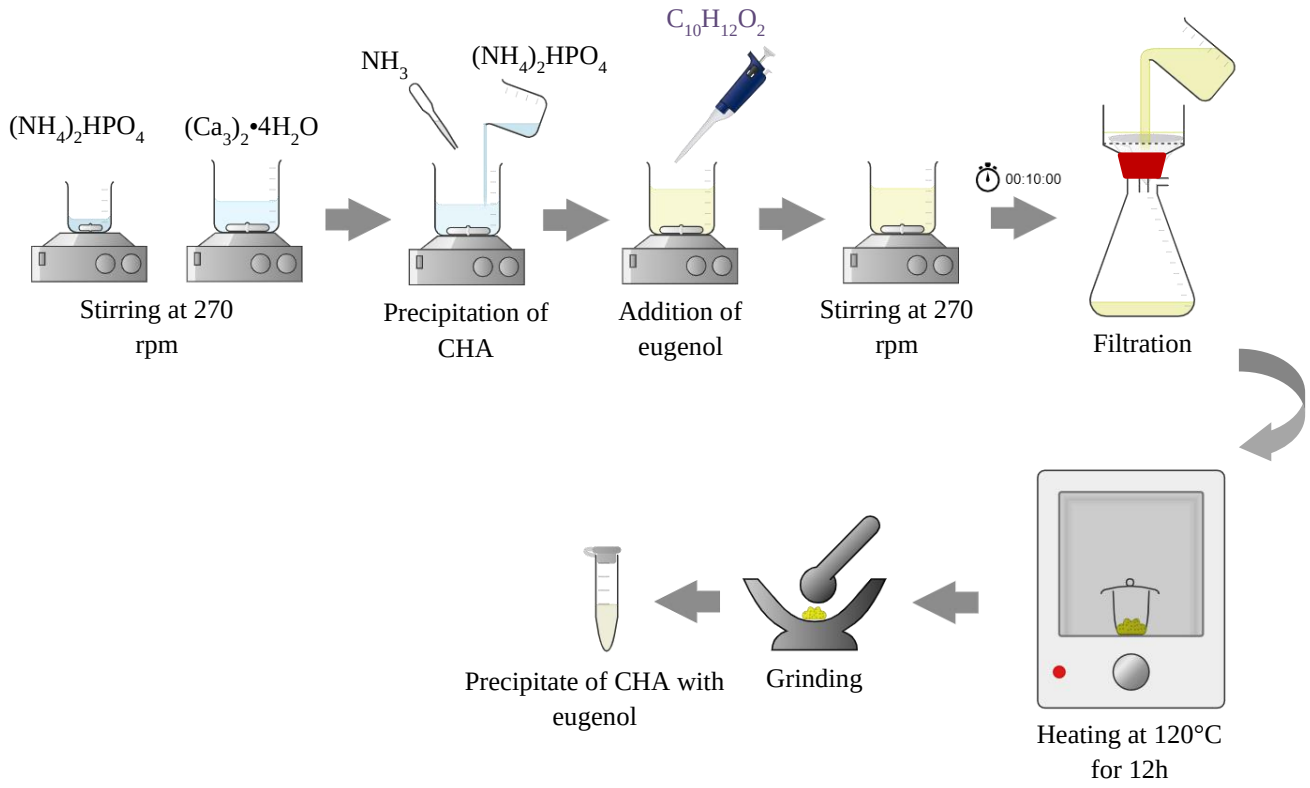

Fig 14. The schematic diagram for the synthesis of CHA/ eugenol composites by the precipitation method

X-ray Diffraction (XRD)

Powder X-ray diffraction (XRD; Rigaku MiniFlex II diffractometer) was analyzed to investigate the synthesized CHA's phase composition. The scanning was performed within the range of 10-60º 2θ at a scanning speed of 10 °/min.

Fourier-Transform Infrared Spectroscopy (FTIR)

Fourier-transform infrared spectroscopy (FTIR; Bruker ALPHA spectrometer) was used to identify the functional groups in the synthesized CHA and CHA/eugenol composites. The FTIR spectra were recorded in the 400–4000 cm^{-1} range with a 4 cm^{-1} resolution.

Thermogravimetric Analysis (TGA)

The thermal decomposition of the materials was conducted using thermogravimetric (TG) analysis, using PerkinElmer STA 6000 for this purpose. 5-10 mg of material was heated from 25ºC to 900ºC at a 10ºC/min heating rate in a nitrogen atmosphere (20 mL/min).

Scanning Electron Microscopy (SEM)

The surface morphologies of the materials were observed using scanning electron microscopy (SEM; Hitachi SU-70 microscope, a Schottky-type field emission electron source).

Brunauer-Emmet-Teller (BET)

The specific surface area of the materials was measured by conducting nitrogen (N_2) gas adsorption via the BET method using a surface area and porosity analyzer, TriStar II 3020.

Chromatography

The quantity of eugenol in the filtrate solutions was determined by a reversed-phase HPLC method using an Agilent 1290 Infinity II LC system (Agilent, Waldbronn, Germany) equipped with a binary pump, thermostatted column compartment, photodiode array detector, and autosampler. Luna Omega C18 (3.0 × 150 mm,3 μm, Phenomenex) column, maintained at 25°C, was used in the experiments. Separations were performed at a 0.5 mL/min flow rate under gradient elution conditions with ACN/H2O mobile phase.

Zone of inhibition test:

Gram-negative *P. aeruginosa* ATCC 15442 and gram-positive *S. aureus* ATCC 29213 were used to test the antibacterial activity of the synthesized materials. Sodium chloride (99%) was obtained from Reachem Slovakia S.r. o (Slovakia). The Gram-positive *Staphylococcus aureus* (ATCC 29213) and Gram-negative *Pseudomonas aeruginosa* (ATCC 15442) were obtained from the Nature Research Centre (Vilnius, Lithuania) collection of microbial strains. The standard microbial growth media, particularly Nutrient Broth (1 g L−1 beef extract, 5 g L−1 peptone, 5 g L−1 sodium chloride, and 2 g L−1 yeast extract, pH=6.8 ± 0.2) and Nutrient agar (1 g L−1 meat extract, 5 g L−1 peptone, 5 g L−1 sodium chloride, 2 g L−1 yeast extract, and 15 g L−1 agar, pH=7.4 ± 0.2), were purchased from Liofilchem (Italy) and used for bacteria propagation, cultivation, and antimicrobial assessments. Milli-Q water (MQ, 18 MΩ·cm) was used to prepare the physiological solution (0.95% NaCl) for diluting bacterial suspensions. The antimicrobial efficiency of the fabricated composites was additionally verified using the modified Kirby-Bauer technique, as described in our previous research [155]. In brief, frozen bacteria cells were seeded on Nutrient agar media and left to grow at 37 °C for 24 h. Then, the few colonies from the bacteria's overnight culture were harvested with an inoculation needle, transferred into the Nutrient Broth media (40 mL), and cultivated at 37 °C (200 rpm) overnight. The newly grown bacteria cells were re-inoculated into liquid media and left to propagate unless the exponential growth phase was

achieved. Cells were collected by centrifugation (2,504×g), double-washed, and resuspended in 0.9% sodium chloride solution. For the zone inhibition approach, the bacteria's suspension was prepared by adjusting their OD600 to yield 1–3.5×108 CFU mL−1 inoculum, corresponding to the OD values in the range from 0.22 to 0.125 and 0.08-0.1 for *S. aureus* and *P. aeruginosa*, respectively. Subsequently, 1 mL of a particular bacterium suspension was poured into Petri dishes and, while mixing, overlaid with Nutrient agar medium, cooled to 50 °C, and allowed to harden. Finally, the small pinch of CHA and synthesized composites, namely, 2% EUG and 5% EUG, powders were carefully placed on the recently inoculated agar plates. In the case of liquid positive control (eugenol), the well-diffusion approach was exercised to test their antimicrobial performance. A sterile 6-mm cork-borer was applied to the nutrient agar media to make wells in inoculated A. Lastly, 100 µL of each particular phenol was introduced into the wells. In contrast, the same amount of sterile MQ was poured into the wells as a control. All antimicrobial assessments were performed in triplicate. Notably, pure CHA and plain inoculated Nutrient agar media acted as a negative control. The susceptibility of tested bacteria strains is determined by measuring the clear circular zone of inhibition around the powders/suspensions of synthesized composites and phenols.

XRD was used for phase composition analysis of the synthesized CHA and CHA-EUG composites, and the patterns are displayed in Fig. 15. All samples exhibited XRD patterns identical to those of CHA [156,157], indicating phase purity and consistency among the materials (standard CHA PDF file No. 00-009-0432), shown as vertical lines for comparison.

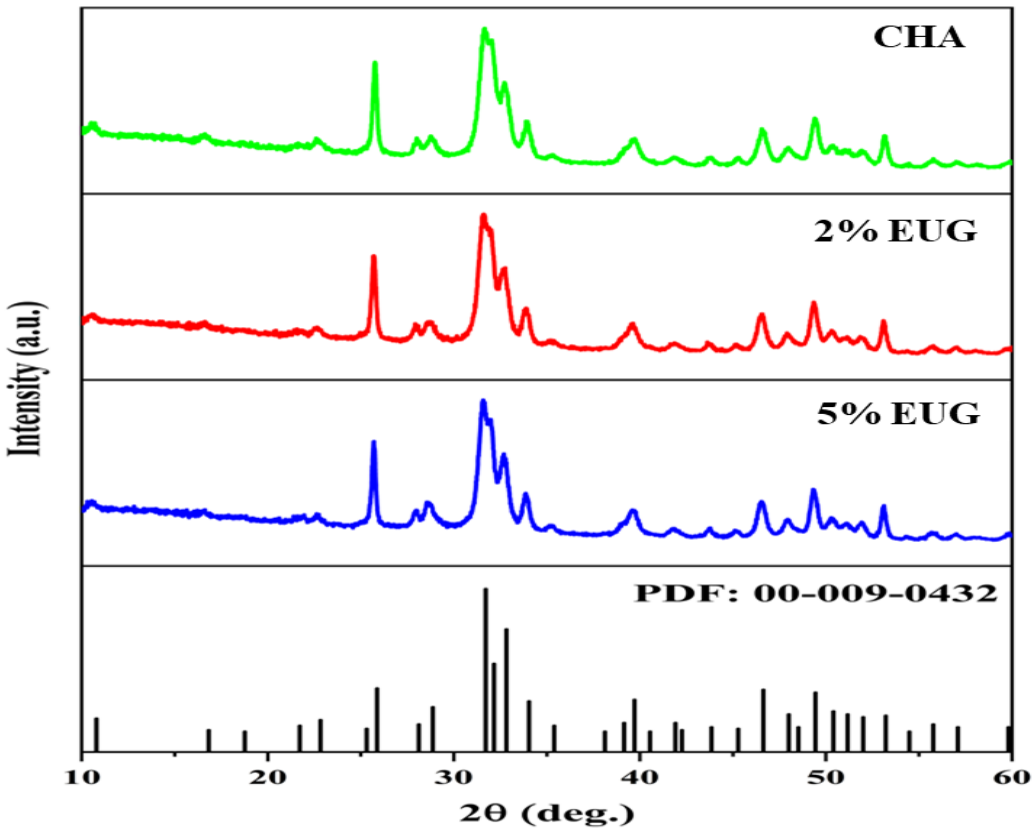

Fig 15. XRD patterns of CHA, 2% EUG, and 5% EUG samples. Vertical lines represent the standard XRD pattern of CHA [PDF: 00-009-0432].

The FTIR spectra of CHA, the obtained composites, and EUG are presented in Fig. 16. The analysis of samples obtained by the precipitation method demonstrates the presence of weak absorption bands at 3571 cm^{-1} and 633 cm^{-1}, which are assigned to the stretching vibration and the bending modes of the hydroxyl group, respectively. The characteristic bands for the phosphate group are detected at 1020-1090 cm^{-1}, 960 cm^{-1}, 560-600 cm^{-1}, and 430-470 cm^{-1} [158]. The bands observed at 1020-1090 cm^{-1} and 960 cm^{-1} are assigned to the phosphate group's asymmetric and symmetric P–O stretching vibrations, respectively. The bands detected in the 560-600 cm^{-1} spectral region are attributed to asymmetric O–P–O bending vibrations, whereas the 430-470 cm^{-1} region corresponds to symmetric O–P–O bending vibrations. A broad absorption band centered at 869 cm^{-1} is assigned to the hydrogen phosphate group's P–O(H) stretching vibration, suggesting a calcium deficiency in the synthesized apatite-type material [159]. The FTIR spectra of the composites exhibit distinct bands at 1428 cm^{-1}, 1328 cm^{-1}, and 824 cm^{-1}, which are absent in the original CHA spectrum. The band at 1428 cm^{-1} is due to C–H in-plane bending in eugenol, while the 1328 cm^{-1} band likely corresponds to Ca^{2+}-phenolate interactions, indicating complex formation between calcium and the phenolic groups. Typically, eugenol exhibits phenolic bending around 1360-1370 cm^{-1}; however, under basic conditions, deprotonation leads to phenolate ion formation and calcium binding, causing the shift to 1328 cm^{-1}. The band observed at 824 cm^{-1} can be attributed to benzene ring vibrations in eugenol molecules. However, when comparing the FTIR spectra of commercial eugenol (Fig. 16), no distinct bands corresponding to organic compounds are observed. This absence may be attributed to the temperature conditions used in this study (120 ºC), which could have induced the absence of their characteristic functional groups.

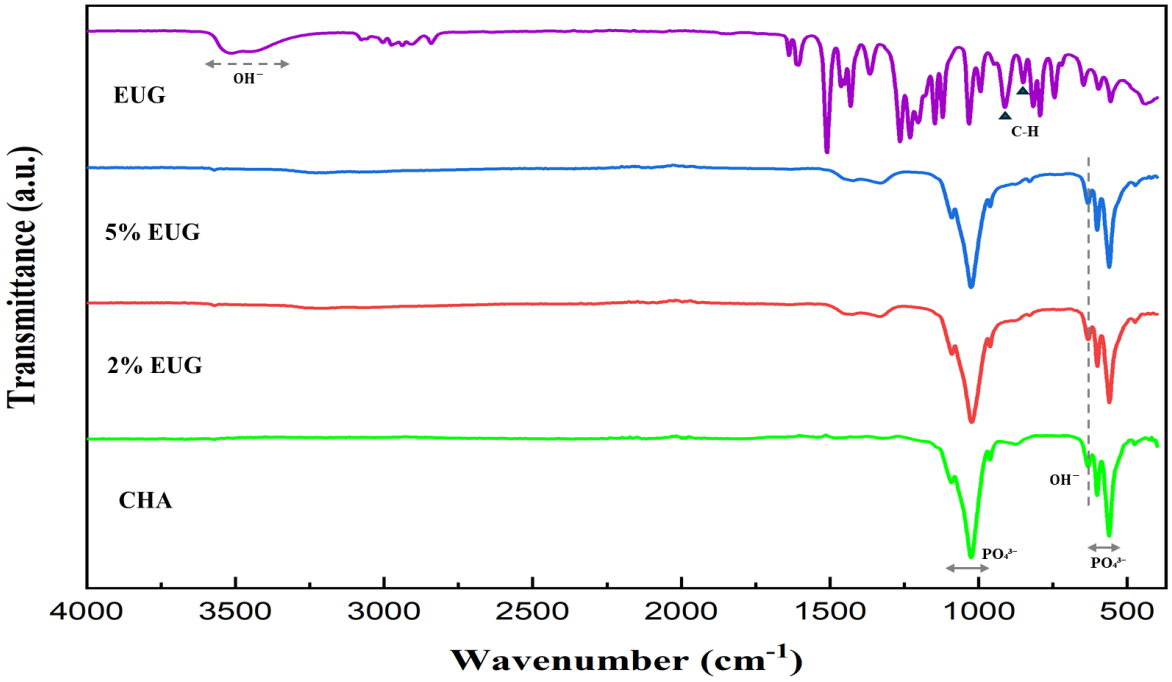

Fig 16. FTIR spectra of CHA, 2% EUG, 5% EUG samples, and pure EUG.

The thermal behavior of CHA and the resulting composites, analyzed through TGA and depicted in Fig. 17, revealed three distinct stages of thermal decomposition. The first weight loss in the CHA sample, synthesized through a precipitation method, occurs when heated between 30 ºC and about 160 ºC. This loss results from the release of absorbed water and moisture from the sample. At this stage, the weight loss in pure CHA and the composites showed no notable differences, indicating that the dehydration process for the composites closely mirrors that of pure CHA. The second stage, occurring from 160 ºC to 730 ºC, relates to the combustion of the organic components in the prepared composites [160]. Pure CHA lost 3.5% of its weight. In contrast, the 2% EUG composite displayed more considerable thermal degradation, with a weight loss of 8.3%. The thermal degradation curve in Fig. 17 highlights a more pronounced weight loss for the 5% EUG sample, which reached 14.7%, suggesting that this composite contains a higher concentration of organic compounds than the others synthesized. The third decomposition stage occurs between 730 °C and 780 °C, associated with the dehydration and decomposition of apatite into β-tricalcium phosphate and the release of water [161]. This stage was similar for all composites, showing minimal weight loss followed by stability until the measurement concluded at 900 ºC.

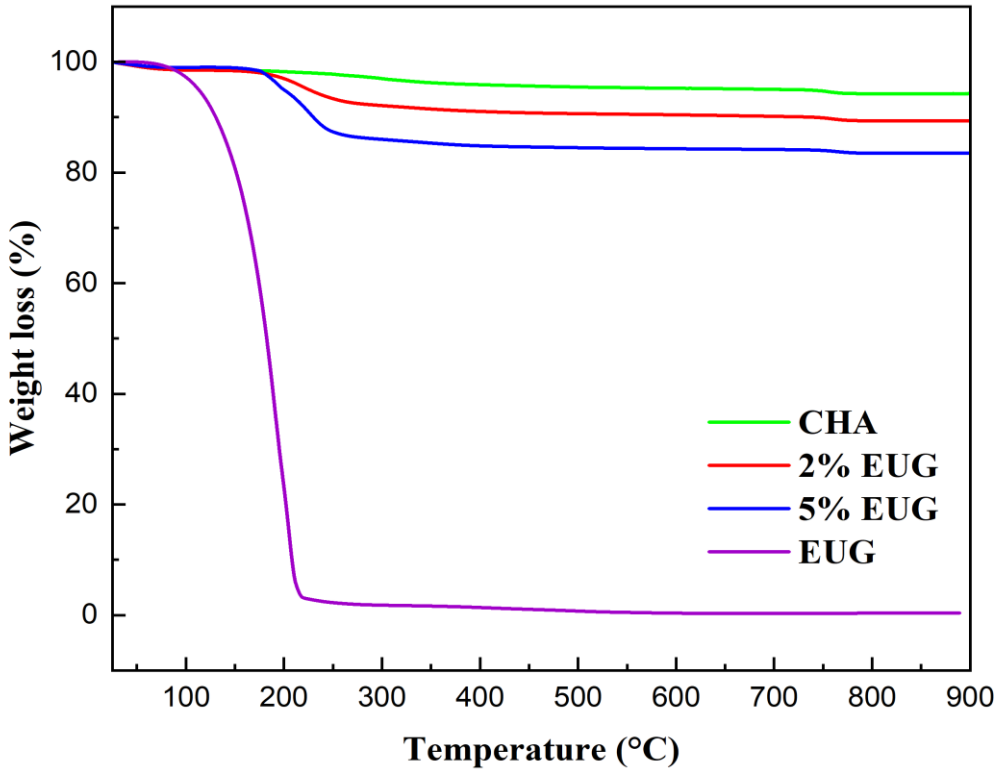

Fig 17. TG analysis curves of CHA, 2% EUG, and 5% EUG samples.

Representative SEM micrographs demonstrate that the surface morphology of CHA and composites is somewhat similar, as shown in Fig. 18. The surface of the CHA is composed of plate-like particles, less than 1 μm in size, which are interconnected to form a network of crystallites. In the case of composites, the formation of elongated particles at approximately 100-200 nm in size, along with plate-like ones, has been observed. Eugenol is distributed uniformly in the composites, and no indications of segregation or the formation of ambiguous particle clusters have been observed; furthermore, the precipitation method results in the formation of nano- and micropores within the composites.

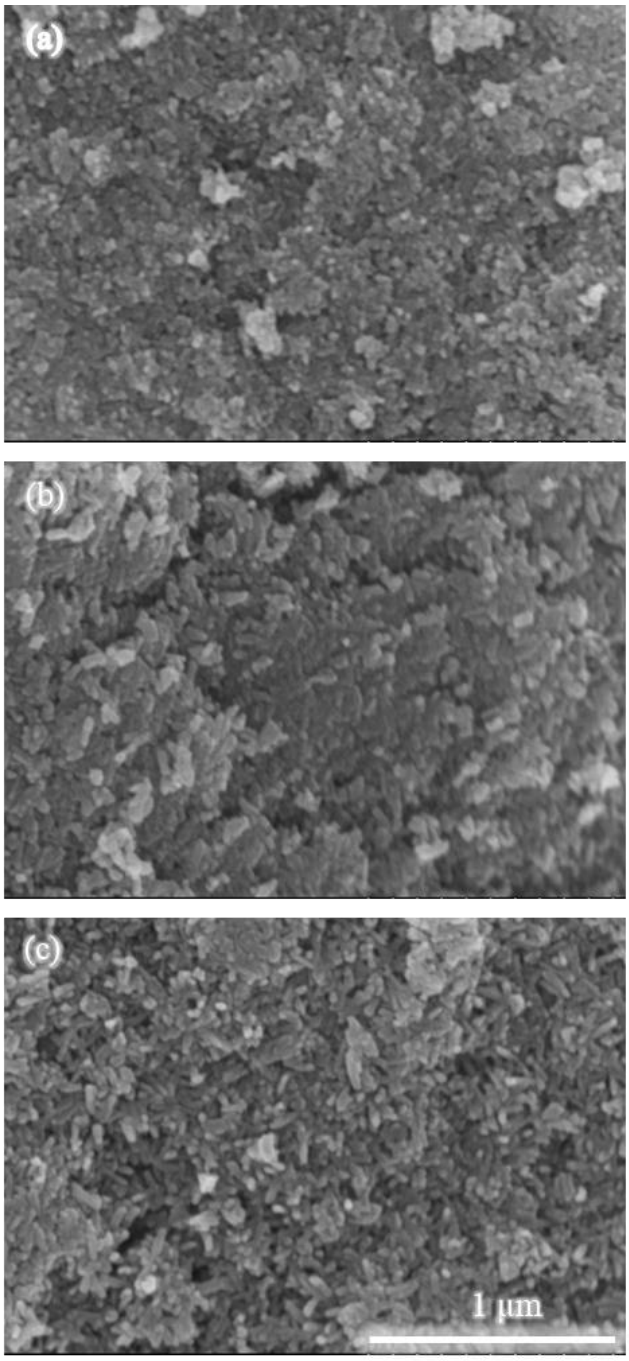

Fig 18. SEM images of CHA (a), 2% EUG (b), and 5% EUG (c) samples.

The obtained composites displayed type IV N2 adsorption-desorption isotherms, indicating the formation of mesoporous structures, and an H3 hysteresis loop [162] with no significant differences between the materials, as shown in Fig. 19. The BET-specific surface area (SBET) of the synthesized materials showed no considerable difference, as presented in Table 2.

The findings demonstrated that the incorporation of eugenol exerted a negligible influence on the surface area of the composites.

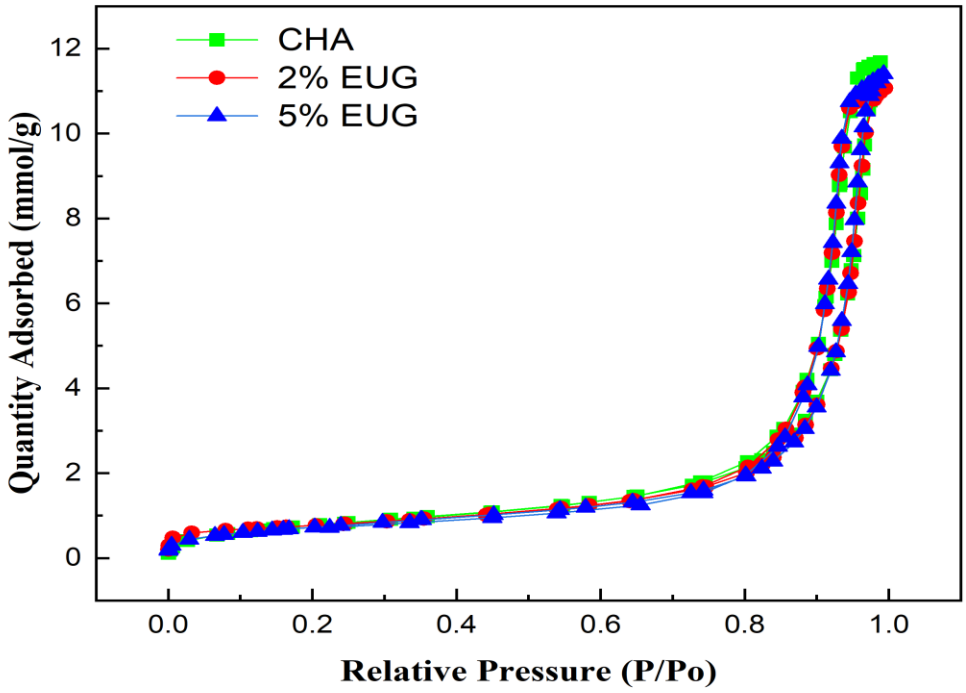

Fig 19. The N_2 adsorption-desorption isotherm of CHA, 2% EUG, and 5% EUG samples.

Table 2. S_{BET} of CHA, 2% EUG, and 5% EUG samples.

Sample	S_{BET} (m^2/g)
CHA	60.40
2% EUG	60.44
5% EUG	60.42

FTIR spectroscopy and TGA analysis qualitatively proved the formation of CHA composites with eugenol. To quantify the content of eugenol in the synthesized composites, the amount of these organic substances was determined chromatographically in the washing solutions (filtrates). Table 3 shows the chromatography results for the synthesized composites. The quantification of organic components via HPLC of the filtrates demonstrated minimal loss, with nearly complete retention in the composites. The determined amounts closely matched the nominal values, indicating efficient incorporation of eugenol into the CHA matrix, where they are chemically bonded to the CHA structure and likely physically adsorbed on the surface or trapped within the pores.

Table 3. Determination of retained eugenol content in CHA composites by reversed-phase HPLC method.

Sample	Concentration in filtrate, mg/L	Nominal amount in composite, g	Determined amount in filtrate, mg	Actual amount in composite, g
CHA	0	0	0	0
2% EUG	888	2	17.76	1.982
5% EUG	913	5	18.26	4.982

3.2.2 Antibacterial Properties

The antibacterial activity of the composites was evaluated against *Staphylococcus aureus* ATCC 29213 and *Pseudomonas aeruginosa* ATCC 15442. It was concluded that phenol-containing EUG composite powders exhibited more efficient antibacterial properties against the Gram-positive *S. aureus* bacteria, possessing a length of the zone ranging from 0.3±0.2 to 0.5±0.1 mm for EUG 2% and EUG 5%, respectively, when compared with CHA, which had a zone length of 0.0±0.0 (Table 4), consequently demonstrating a concentration-dependent bactericidal effect, as shown in Fig. 20 (a).

In contrast, in the case of Gram-negative *P. aeruginosa* bacteria, the length of the lysis zone was concentration independent, with all tested composite powders possessing only bacteriostatic activity Fig. 20 (b). Moreover, pure CHA possessed comparable bacteriostatic activity on the lawns of *P. aeruginosa* (Fig. 20 b). However, no effect was obtained with *S. aureus* cells, indicating that CHA does not exhibit broad-spectrum antibacterial activity. Thus, further functionalization is necessary to enhance its antimicrobial properties Fig. 20 (a).

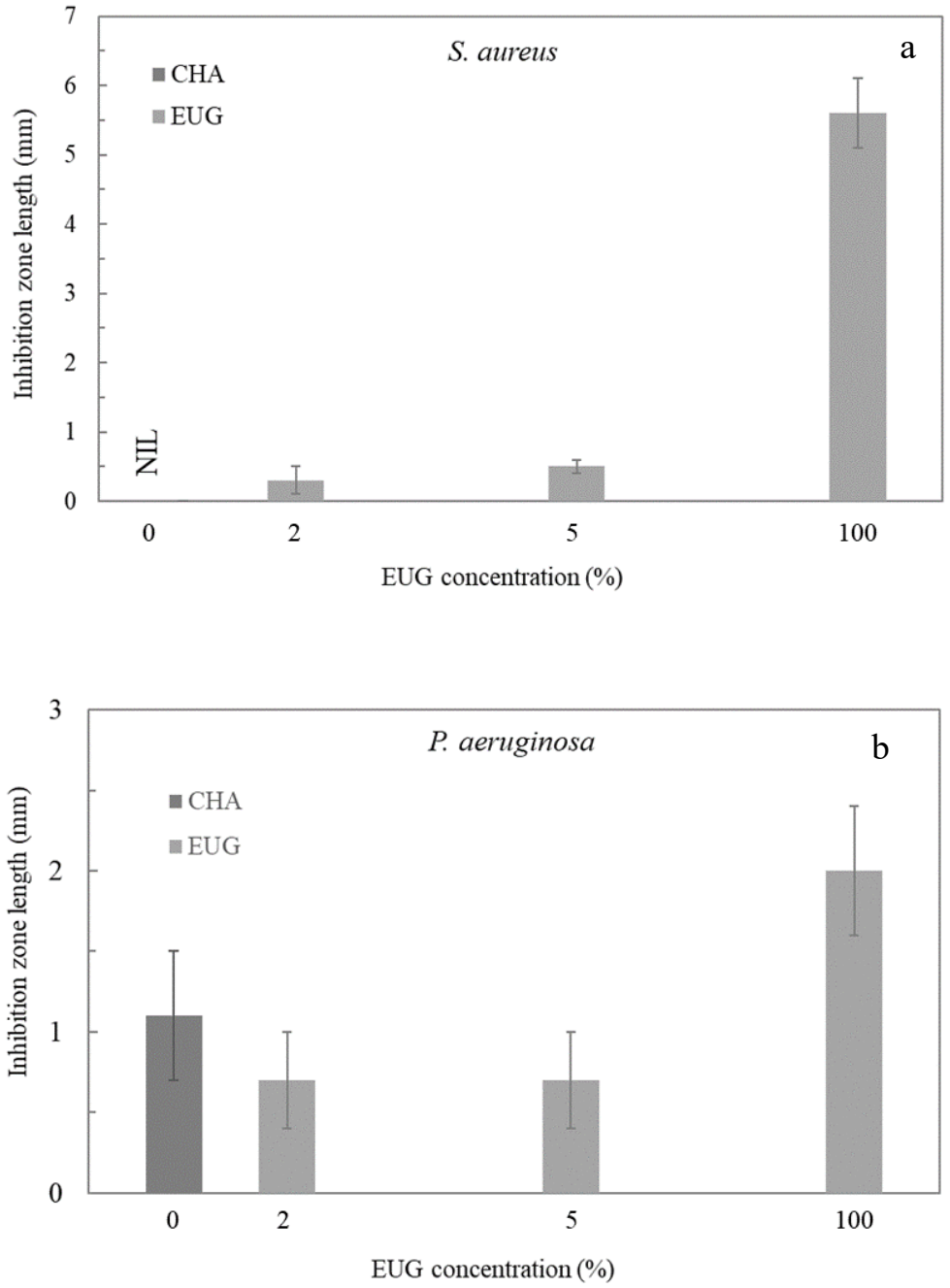

Fig 20. Concentration-dependent antimicrobial activity of the composite comprised of CHA with different concentrations of eugenol towards inhibiting *S. aureus* ATCC 29213 (a) and *P. aeruginosa* ATCC 15442 (b) growth.

Table 4. The antimicrobial activity of CHA, 2% EUG, 5% EUG composite powder, and pure eugenol against Gram-positive *S. aureus* ATCC 29213 bacteria and Gram-negative *P. aeruginosa* ATCC 15442.

Antimicrobial agent	Microorganism	Averaged length of inhibition zone, mm	Effect
CHA	*S. aureus*	0.0±0.0	*
2% EUG		0.3±0.2	Bacteriostatic
5% EUG		0.5±0.1	
Eugenol		5.6±0.5	
CHA	*P. aeruginosa*	1.1±0.4	
2% EUG		0.7±0.3	
5% EUG		0.7±0.3	
Eugenol		2.0±0.4	Bactericidal

*-there is no effect and/or it is impossible to evaluate.

CHA composites containing eugenol are promising candidates for antibacterial applications, considering several factors that might influence their effectiveness, such as concentration of organic constituents, their morphological structures, and the targeted species of bacteria.
This combination could exhibit synergistic effects by enhancing the bioactivity while reducing cytotoxicity, as both eugenol and isoeugenol are generally safe at low concentrations and can only be cytotoxic at high concentrations [163]. Thus, the obtained composites are promising materials for biomedical and dental applications.

CONCLUSIONS

1. The comparative study presented distinct characteristics of CHA, which were fabricated through sol-gel, hydrothermal, and precipitation techniques. The study focused on the crystallinity, surface morphology, and thermal stability. CHA synthesized using the sol-gel method resulted in highly uniform and fine particles. The XRD confirmed the phase composition and showed the differences in the crystallinity compared to the CHA obtained by hydrothermal and precipitation techniques. Since the sol-gel requires high temperatures for calcination, it improved the thermal stability, as confirmed by the TGA analysis. The FTIR spectra of CHA samples confirmed the presence of the phosphate and hydroxyl functional groups.
2. The formation of CHA and CHA-containing eugenol composites using the environmentally friendly precipitation method. The XRD confirmed the chemical composition. The FTIR spectra confirmed the presence of the phosphate, hydroxyl, and hydrogen phosphate groups in the pure CHA samples. Meanwhile, the composites exhibited C–H in-plane bending in eugenol, and some bands corresponded to Ca^{2+}-phenolate interactions. The TGA analysis revealed more weight loss in the composites of EUG 5% compared to the pure CHA and EUG 2%, suggesting a higher amount of organic compounds in the composition of EUG 5%. Incorporating eugenol into the CHA improved the antibacterial properties against Gram-positive (*S. aureus*) bacteria when compared with CHA samples without eugenol incorporation.

SUMMARY IN LITHUANIAN

Šiame magistro darbe pateikiamas trijų kalcio hidroksiapatito $Ca_{10}(PO_4)_6(OH)_2$; CHA) sintezės metodų lyginamasis tyrimas: sol-gelio, hidroterminės ir nusodinimo technikos. Tikslas buvo įvertinti, kaip kiekvienas metodas veikia CHA struktūrines ir morfologines savybes, ir ištirti jo kompozitų su eugenoliu antibakterinį aktyvumą. Rezultatai parodė, kad sol-gelio metodas gamina didžiausią kristališkumą ir terminį stabilumą turintį CHA. Taikant hidroterminį metodą buvo gauti tiksliai apibrėžti vidutinio stabilumo kristalai, o nusodinimo metodas, nors ir paprastas ir ekonomiškas, lėmė ne tokias vienodas daleles. Vėliau CHA-eugenolio kompozitai buvo susintetinti naudojant nusodinimo metodą ir apibūdinti naudojant įvairius analitinius metodus. Antibakterinė analizė parodė, kad šių kompozitų antibakterinis aktyvumas prieš gramteigiamą Staphylococcus aureus, palyginti su gramneigiamu Pseudomonas aeruginosa, buvo stipresnis. Šie rezultatai rodo, kad CHA-eugenolio kompozitai turi daug žadančio potencialo dantų ir biomedicinos srityse.

This Master's thesis presents a comparative study of three synthesis methods for calcium hydroxyapatite ($Ca_{10}(PO_4)_6(OH)_2$; CHA): sol-gel, hydrothermal, and precipitation techniques. The aim was to evaluate how each method affects the structural and morphological properties of CHA and to investigate the antibacterial activity of its composites with eugenol. The results demonstrated that the sol-gel method produced CHA with the highest crystallinity and thermal stability. The hydrothermal method yielded well-defined crystals with moderate stability, while the precipitation method, though simple and cost-effective, resulted in less uniform particles. Subsequently, CHA-eugenol composites were synthesized using the precipitation method and characterized using various analytical techniques. The antibacterial analysis revealed that these composites exhibited enhanced antibacterial activity against the Gram-positive Staphylococcus aureus, compared to the Gram-negative Pseudomonas aeruginosa. These findings suggest that CHA-eugenol composites have promising potential in dental and biomedical applications.

ACKNOWLEDGMENT

I would like to sincerely thank my supervisor, **Prof. Habil. Dr. Aivaras Kareiva**, for his constant support, expert advice, and patience throughout the course of my thesis. His guidance helped me develop a deeper understanding of scientific research and critical analysis. I am also very grateful to **Assoc. Prof. Dr. Živilė Stankevičiūtė** for her thoughtful feedback and encouragement during the development of this work.

My special thanks go to **Dr. Maab Abdulsamad Ahmed Elsheikh** for her valuable insights and for always being approachable whenever I needed clarification or support. Her experience and kind mentorship had a strong influence on the successful completion of this project.

I would also like to acknowledge the entire **Department of Inorganic Chemistry** at Vilnius University for providing the necessary resources and a supportive academic environment. The staff and fellow students contributed greatly through helpful discussions and collaboration.

Most importantly, I would like to express my heartfelt gratitude to my **parents** for their unconditional love, constant encouragement, and sacrifices that made this journey possible. Their unwavering belief in me has been my greatest source of motivation and strength throughout my academic path.

REFERENCES:

[1] J. Wüster, N. Neckel, F. Sterzik, L. Xiang-Tischhauser, D. Barnewitz, A. Genzel, S. Koerdt, C. Rendenbach, C. Müller-Mai, M. Heiland, S. Nahles, C. Knabe, Effect of a synthetic hydroxyapatite-based bone grafting material compared to established bone substitute materials on regeneration of critical-size bone defects, Regener. Biomater. 10 (2023) rbae041. https://doi.org/10.1093/rb/rbae041.

[2] National Center for Biotechnology Information (NCBI), Hydroxyapatite bioceramics, (2023). https://www.ncbi.nlm.nih.gov/books/NBK513314/.

[3] H. Shi, Z. Zhou, W. Li, Y. Fan, Z. Li, J. Wei, Hydroxyapatite-based materials for bone tissue engineering: A brief and comprehensive introduction, Crystals 11 (2021) 149. https://doi.org/10.3390/cryst11020149.

[4] K. Matsuno, N. Yamada, A. Morimoto, M. Sakurai, Bioactivity of hydroxyapatite: Applications in biomedical fields, Biomater. Res. 22 (2018) 31. https://doi.org/10.1186/s40824-018-0149-3.

[5] S. Torres-Romero, A. Mendoza-Acosta, M.R. Flores-Cortez, F. Gamez-Serna, A.S. Váldez-Robles, C.A. Soto-Robles, Hydroxyapatite production techniques: Overview of precipitation, sol–gel, hydrothermal, and thermal decomposition methods, IOSR J. Appl. Chem. 17 (2024) 56–64. https://www.iosrjournals.org/iosr-jac/papers/vol17-issue1/Ser-1/G1701015664.pdf.

[6] I. Ielo, G. Calabrese, G. De Luca, S. Conoci, Recent advances in hydroxyapatite-based biocomposites for bone tissue regeneration in orthopedics, Int. J. Mol. Sci. 23 (2022) 9721. https://doi.org/10.3390/ijms23179721.

[7] M.B. Conz, J.M. Granjeiro, G.A. Soares, Hydroxyapatite crystallinity does not affect the repair of critical size bone defects, J. Appl. Oral Sci. 19 (2011) 337–342. https://doi.org/10.1590/S1678-77572011005000007.

[8] M. Prakash, H.K. Rajan, M.N. Chandraprabhaa, Recent developments in green synthesis of hydroxyapatite nanocomposites: Relevance to biomedical and environmental applications, Green Chem. Lett. Rev. 17 (2024) 1–20. https://doi.org/10.1080/17518253.2024.2422409.

[9] M. Ulanowska, B. Olas, Biological properties and prospects for the application of eugenol: A review, Int. J. Mol. Sci. 22 (2021) 3671. https://doi.org/10.3390/ijms22073671.

[10] M.F. Nisar, M. Khadim, M. Rafiq, J. Chen, Y. Yang, C.C. Wan, Pharmacological properties and health benefits of eugenol: A comprehensive review, Oxid. Med. Cell. Longev. (2021) 2497354. https://doi.org/10.1155/2021/2497354.

[11] M. Hyldgaard, T. Mygind, R. Piotrowska, M. Foss, R.L. Meyer, Isoeugenol has a non-disruptive detergent-like mechanism of action, Front. Microbiol. 6 (2015) 754. https://doi.org/10.3389/fmicb.2015.00754.

[12] A.F. Vladu, S. Marin, I.A. Neacșu, R.D. Trușcă, M.G. Albu Kaya, D.A. Kaya, A.M. Popa, C. Poiană, I. Cristescu, Spongious fillers based on collagen-hydroxyapatite-eugenol acetate with therapeutic potential in bone cancer, Farmacia 68 (2020) 313–321.

[13] T. Windarti, N.B.A. Prasetya, Ngadiwiyana, L.N. Nulandaya, Calcium phosphate cement composed of hydroxyapatite modified silica and polyeugenol as a bone filler material, Indones. J. Chem. 23 (2023) 313–321. https://doi.org/10.22146/ijc.80298.

[14] A.A. Vu, S. Bose, Natural antibiotic oregano in hydroxyapatite-coated titanium reduces osteoclastic bone resorption for orthopedic and dental applications, ACS Appl. Mater. Interfaces 12 (2020) 52383–52392. https://doi.org/10.1021/acsami.0c14993.
[15] R.M. Jagtap, V.S. Nandre, D.R. Kshirsagar, K.M. Kodam, S.K. Pardeshi, Mechanochemically processed silver-decorated ZnO-eugenol composite nanocrystallites and their dual bactericidal modes, Mater. Res. Bull. 118 (2019) 110503. https://doi.org/10.1016/j.materresbull.2019.110503.
[16] M. Mansoorianfar, M. Mansourianfar, M. Fathi, S. Bonakdar, M. Ebrahimi, E.M. Zahrani, A. Hojjati-Najafabadi, D. Li, Surface modification of orthopedic implants by optimized fluorine-substituted hydroxyapatite coating: Enhancing corrosion behavior and cell function, Ceram. Int. 46 (2020) 2139–2146. https://doi.org/10.1016/j.ceramint.2019.09.197.
[17] J.F. Hui, G.L. Xiang, X.X. Xu, J. Zhuang, X. Wang, Monodisperse F-substituted hydroxyapatite single-crystal nanotubes with amphiphilic surface properties, Inorg. Chem. 48 (2009) 5614–5616. https://doi.org/10.1021/ic900697b.
[18] D. Knaack, M.E.P. Goad, M. Aiolova, C. Rey, A. Tofighi, P. Chakravarthy, D. Lee, Resorbable calcium phosphate bone substitute, J. Biomed. Mater. Res. 43 (1998) 399–409. https://doi.org/10.1002/(SICI)1097-4636(199824)43:4<399::AID-JBM7>3.0.CO;2-J.
[19] E. Landi, G. Celotti, G. Logroscino, A. Tampieri, Carbonated hydroxyapatite as bone substitute, J. Eur. Ceram. Soc. 23 (2003) 2931–2937. https://doi.org/10.1016/S0955-2219(03)00304-2.
[20] S.S. Kim, M.S. Park, O. Jeon, C.Y. Choi, B.S. Kim, Poly(lactide-co-glycolide)/hydroxyapatite composite scaffolds for bone tissue engineering, Biomaterials 27 (2006) 1399–1409. https://doi.org/10.1016/j.biomaterials.2005.08.016.
[21] M. Gruselle, Apatites: A new family of catalysts in organic synthesis, J. Organomet. Chem. 793 (2015) 93–101. https://doi.org/10.1016/j.jorganchem.2015.01.018.
[22] Y. Mizushima, T. Ikoma, J. Tanaka, K. Hoshi, T. Ishihara, Y. Ogawa, A. Ueno, Injectable porous hydroxyapatite microparticles as a new carrier for protein and lipophilic drugs, J. Control. Release 110 (2006) 260–265. https://doi.org/10.1016/j.jconrel.2005.09.051.
[23] Z. Xia, L. Liao, S. Zhao, Synthesis of mesoporous hydroxyapatite using a modified hard-templating route, Mater. Res. Bull. 44 (2009) 1626–1629. https://doi.org/10.1016/j.materresbull.2009.04.014.
[24] J.C. Elliott, Structure and Chemistry of the Apatites and Other Calcium Orthophosphates, Elsevier, Amsterdam, The Netherlands, 1994. https://doi.org/10.1016/c2009-0-10247-7.
[25] M. Šupová, Substituted hydroxyapatites for biomedical applications: A review, Ceram. Int. 41 (2015) 9203–9231. https://doi.org/10.1016/j.ceramint.2015.03.316.
[26] T.J. White, D. Zhili, Structural derivation and crystal chemistry of apatites, Acta Crystallogr. B 59 (2003) 1–16. https://doi.org/10.1107/S0108768102019894.
[27] J.T.B. Ratnayake, M. Mucalo, G.J. Dias, Substituted hydroxyapatites for bone regeneration: A review of current trends, J. Biomed. Mater. Res. B 105 (2017) 1285–1299. https://doi.org/10.1002/jbm.b.33651.
[28] S. Ezhaveni, R. Yuvakkumar, M. Rajkumar, N.M. Sundaram, V. Rajendran, Preparation and characterization of nano-hydroxyapatite nanomaterials for liver cancer cell treatment, J. Nanosci. Nanotechnol. 13 (2013) 1631–1638. https://doi.org/10.1166/jnn.2013.7135.

[29] S. Kang, H. Kim, Y. Lee, I.K. Kang, Hydroxyapatites as bone grafts and coating materials in dental science, Mod. Res. Dent. 7 (2022) 757–764. https://doi.org/10.31031/MRD.2022.07.000668.
[30] K. Lin, L. Chen, J. Chang, Fabrication of dense hydroxyapatite nanobioceramics with enhanced mechanical properties via a two-step sintering process, Int. J. Appl. Ceram. Technol. 9 (2012) 479–485. https://doi.org/10.1111/j.1744-7402.2011.02654.x.
[31] B.C.H. Steele, Material science and engineering: The enabling technology for commercializing fuel cell systems, J. Mater. Sci. 36 (2001) 1053–1068. https://doi.org/10.1023/A:1004853019349.
[32] E.M. Rivera, M. Araiza, W. Brostow, V.M. Castano, J.R. Díaz-Estrada, R. Hernandez, J.R. Rodríguez, Synthesis of hydroxyapatite from eggshells, Mater. Lett. 41 (1999) 128–134. https://doi.org/10.1016/S0167-577X(99)00118-4.
[33] S.J. Lee, S.H. Oh, Fabrication of calcium phosphate bioceramics by using eggshell and phosphoric acid, Mater. Lett. 57 (2003) 4570–4574. https://doi.org/10.1016/S0167-577X(03)00363-X.
[34] C. Balazsi, F. Weber, Z. Köver, E. Horvath, C. Nameth, Preparation of calcium-phosphate bioceramics from natural resources, J. Eur. Ceram. Soc. 27 (2007) 1601–1606. https://doi.org/10.1016/j.jeurceramsoc.2006.04.016.
[35] K.S. Vecchio, X. Zhang, J.B. Massie, M. Wang, C.W. Kim, Conversion of bulk seashells to biocompatible hydroxyapatite for bone implants, Acta Biomater. 3 (2007) 910–918. https://doi.org/10.1016/j.actbio.2007.06.003.
[36] U. Ripamonti, J. Crooks, L. Khoali, L. Roden, The induction of bone formation by coral-derived calcium carbonate/hydroxyapatite constructs, Biomaterials 30 (2009) 1428–1439. https://doi.org/10.1016/j.biomaterials.2008.10.065.
[37] W. Khoo, F.M. Nor, H. Ardhyananta, D. Kurniawan, Preparation of natural hydroxyapatite from bovine femur bones using calcination at various temperatures, Procedia Manuf. 2 (2015) 196–201. https://doi.org/10.1016/j.promfg.2015.07.034.
[38] R.O. Kareem, N. Bulut, O. Kaygili, Hydroxyapatite biomaterials: A comprehensive review of their properties, structures, medical applications, and fabrication methods, J. Chem. Rev. 6 (2024) 1–26. https://doi.org/10.48309/JCR.2024.415051.1253.
[39] K. Labgairi, A. Borji, M. Kaddami, A. Jourani, Kinetic study of calcium phosphate precipitation in the system H_3PO_4–$Ca(OH)_2$–H_2O at 30°C, Int. J. Chem. Eng. (2020) 2893298. https://doi.org/10.1155/2020/2893298.
[40] M. Trzaskowska, V. Vivcharenko, A. Przekora, The impact of hydroxyapatite sintering temperature on its microstructural, mechanical, and biological properties, Int. J. Mol. Sci. 24 (2023) 5083. https://doi.org/10.3390/ijms24065083.
[41] L. Bandeira, P. Calefi, K. Ciuffi, E. Nassar, I. Salvado, M. Fernandes, Low temperature synthesis of bioactive materials, Cerâmica 57 (2011) 166–172. https://doi.org/10.1590/S0366-69132011000200006.
[42] C.S. Chai, B. Ben-Nissan, Bioactive nanocrystalline sol–gel hydroxyapatite coatings, J. Mater. Sci. Mater. Med. 10 (1999) 465–469. https://doi.org/10.1023/A:1008992807888.
[43] S.A. Manafi, B. Yazdani, M.R. Rahimiopour, S.K. Sadrnezhaad, M.H. Amin, M. Razavi, Synthesis of nano-hydroxyapatite under a sonochemical/hydrothermal condition, Biomed. Mater. 3 (2008) 025002. https://doi.org/10.1088/1748-6041/3/2/025002.

[44] M.H. Santos, M. de Oliveira, P. de Freitas Souza, H.S. Mansur, W.L. Vasconcelos, Synthesis control and characterization of hydroxyapatite prepared by wet precipitation process, Mater. Res. 7 (2004) 625–630. https://doi.org/10.1590/S1516-14392004000400017.
[45] C.M. Manuel, M.P. Ferraz, F.J. Monteiro, Nanoapatite and microporous structures of hydroxyapatite, Proc. 17th Eur. Soc. Biomater. (2002) T153.
[46] C.M. Manuel, M.P. Ferraz, F.J. Monteiro, Synthesis of hydroxyapatite and tricalcium phosphate nanoparticles: Preliminary studies, Key Eng. Mater. 240–242 (2003) 555–558. https://doi.org/10.4028/www.scientific.net/KEM.240-242.555.
[47] A. Balamurugan, J. Michel, J. Faure, H. Benhayoune, L. Wortham, G. Sockalingum, V. Banchet, S. Bouthors, D. Laurent-Maquin, G. Balossier, Synthesis and structural analysis of sol–gel derived stoichiometric monophasic hydroxyapatite, Ceram. Silik. 50 (2006) 27–31. https://doi.org/10.1016/j.matlet.2006.03.102.
[48] Y. Masuda, K. Matubara, S. Sakka, Synthesis of hydroxyapatite from metal alkoxides through sol–gel technique, J. Ceram. Soc. Jpn. 98 (1990) 1266–1277. https://doi.org/10.2109/jcersj.98.1255.
[49] P. Li, K. de Groot, Better bioactive ceramics through sol–gel process, J. Sol-Gel Sci. Technol. 2 (1994) 797–801. https://doi.org/10.1007/BF00486353.
[50] F. Pena-Pereira, R.M. Duarte, A.C. Duarte, Immobilization strategies and analytical applications for metallic and metal-oxide nanomaterials on surfaces, Trends Anal. Chem. 40 (2012) 90–105. https://doi.org/10.1016/j.trac.2012.07.015.
[51] T. Brendel, A. Engel, C. Russel, Hydroxyapatite coating by polymeric route, J. Mater. Sci. Mater. Med. 3 (1992) 175–179. https://doi.org/10.1007/BF00713445.
[52] D.B. Haddow, P.F. James, R. Van Noort, Characterization of sol–gel surfaces for biomedical applications, J. Mater. Sci. Mater. Med. 7 (1996) 255–260. https://doi.org/10.1007/BF00058562.
[53] D. Gomes, A. Santos, G. Neves, R. Menezes, A brief review on hydroxyapatite production and use in biomedicine, Cerâmica 65 (2019) 282–302. https://doi.org/10.1590/0366-69132019653742706.
[54] R. Karalkeviciene, E. Raudonyte-Svirbutaviciene, A. Zarkov, J.C. Yang, A.I. Popov, A. Kareiva, Solvothermal synthesis of calcium hydroxyapatite via hydrolysis of alpha-tricalcium phosphate in the presence of different organic additives, Crystals 13 (2023) 265. https://doi.org/10.3390/cryst13020265.
[55] G. Huang, C. Lu, H. Yang, Magnetic nanomaterials for magnetic bioanalysis, in: Magnetic Nanomaterials for Magnetic Bioanalysis, Elsevier Inc., 2019, Chapter 3. https://doi.org/10.1016/B978-0-12-814497-8.00003-5.
[56] Y. Qi, J. Shen, Q. Jiang, B. Jin, J. Chen, X. Zhang, The morphology control of hydroxyapatite microsphere at high pH values by hydrothermal method, Adv. Powder Technol. 26 (2015) 1041–1046. https://doi.org/10.1016/j.apt.2015.04.008.
[57] Y. Wang, X. Ren, X. Ma, W. Su, Y. Zhang, X. Sun, X. Li, Design, alginate-intervened hydrothermal synthesis of hydroxyapatite nanocrystals with nanopores, Cryst. Growth Des. 15 (2015) 1949–1956. https://doi.org/10.1021/acs.cgd.5b00113.
[58] G. Zhang, J. Chen, S. Yang, Q. Yu, Z. Wang, Q. Zhang, Preparation of amino-acid-regulated hydroxyapatite particles by hydrothermal method, Mater. Lett. 65 (2011) 572–574. https://doi.org/10.1016/j.matlet.2010.10.078.

[59] S.L. Ortiz, J.H. Avila, M.P. Gutierrez, H. Gomez-Pozos, Hydrothermal synthesis and characterization of hydroxyapatite microstructures, in: 14th Int. Conf. Electr. Eng. Comput. Sci. Autom. Control, 2017. https://doi.org/10.1109/iceee.2017.8108902.
[60] Y. Wang, Y. Zhang, K. Wei, N. Zhao, J. Chen, X. Wang, Hydrothermal synthesis of hydroxyapatite nanopowders using cationic surfactant as a template, Mater. Lett. 60 (2006) 1484–1487. https://doi.org/10.1016/j.matlet.2005.11.053.
[61] R.O. Nagata, Y. Yamauchi, M. Tomita, K. Kato, Hydrothermal synthesis of hydroxyapatite nanoparticles and their protein adsorption behavior, J. Ceram. Soc. Jpn. 121 (2013) 797–801. https://doi.org/10.2109/jcersj2.121.797.
[62] T.T. Hoai, N.K. Nga, L.T. Giang, et al., Hydrothermal synthesis of hydroxyapatite nanorods for rapid formation of bone-like mineralization, J. Electron. Mater. 46 (2017) 5064–5072. https://doi.org/10.1007/s11664-017-5509-6.
[63] Y. Qi, J. Shen, Q. Jiang, B. Jin, J. Chen, X. Zhang, The morphology control of hydroxyapatite microsphere at high pH values by hydrothermal method, Adv. Powder Technol. 26 (2015) 1041–1046. https://doi.org/10.1016/j.apt.2015.04.008.
[64] L. Kong, J. Ma, F. Boey, Nanosized hydroxyapatite powders derived from coprecipitation process, J. Mater. Sci. 37 (2002) 1131–1134. https://doi.org/10.1023/A:1014355103125.
[65] S. Catros, F. Guillemot, E. Lebraud, C. Chanseau, S. Perez, R. Bareille, J. Amédée, J.C. Fricain, Physico-chemical and biological properties of a nano-hydroxyapatite powder synthesized at room temperature, IRBM 31 (2010) 226–233. https://doi.org/10.1016/j.irbm.2010.04.002.
[66] Y.H. Huang, Y.J. Shih, F.J. Cheng, Novel $KMnO_4$-modified iron oxide for effective arsenite removal, J. Hazard. Mater. 198 (2011) 1–6. https://doi.org/10.1016/j.jhazmat.2011.10.010.
[67] A. Afshar, M. Ghorbani, N. Ehsani, M.R. Saeri, C.C. Sorrell, Some important factors in the wet precipitation process of hydroxyapatite, Mater. Des. 24 (2003) 197–202. https://doi.org/10.1016/S0261-3069(03)00003-7.
[68] M. Sadat-Shojai, M.T. Khorasani, E. Dinpanah-Khoshdargi, A. Jamshidi, Synthesis methods for nanosized hydroxyapatite with diverse structures, Acta Biomater. 9 (2013) 7591–7621. https://doi.org/10.1016/j.actbio.2013.04.012.
[69] E. Bouyer, F. Gitzhofer, M.I. Boulos, Morphological study of hydroxyapatite nanocrystal suspension, J. Mater. Sci. Mater. Med. 11 (2000) 523–531. https://doi.org/10.1023/A:1008918110156.
[70] Y.T. Huang, M. Imura, Y. Nemoto, C.H. Cheng, Y. Yamauchi, Block-copolymer-assisted synthesis of hydroxyapatite nanoparticles with high surface area and uniform size, Sci. Technol. Adv. Mater. 12 (2011) 045005. https://doi.org/10.1088/1468-6996/12/4/045005.
[71] M. El-Kholy, A. Khalil, A.M. Hashem, Thermochemistry of bovine teeth and synthesis of hydroxyapatite, Interceram 47 (1998) 29–32.
[72] E.C. da S. Rigo, et al., Synthesis and characterization of hydroxyapatite formed by precipitation process, Mater. Res. 11 (2008) 475–479. https://doi.org/10.1590/S1516-14392008000400016.
[73] S.K. Mohan, R. Sarkar, Reaction sintered zinc oxide incorporated magnesium aluminate spinel from commercial grade oxide reactants, J. Aust. Ceram. Soc. 53 (2017) 207–216. https://doi.org/10.1007/s41779-017-0026-x.

[74] H. Dressman, Ueber Knochenplombierung bei hohlenformigen Defekten des Knochens, Beitr. Klin. Chir. 9 (1892) 804–810.
[75] S.V. Dorozhkin, A history of calcium orthophosphates ($CaPO_4$) and their biomedical applications, Morphologie 101 (2017) 143–153. https://doi.org/10.1016/j.morpho.2017.05.001.
[76] F.H. Albee, Evolution of bone graft surgery, Am. J. Surg. 63 (1944) 421–436. https://doi.org/10.1016/S0002-9610(44)90389-2.
[77] F.H. Albee, Studies in bone growth. Triple calcium phosphate as a stimulus to osteogenesis, Ann. Surg. 71 (1920) 32–39. https://doi.org/10.1097/00000658-192001000-00006.
[78] H. Aoki, K. Kato, M. Ogiso, T. Tabata, Studies on the application of apatite to dental materials, Jpn. Soc. Dent. Mater. Devices 18 (1977) 86–89.
[79] G.L. de Lange, K. Donath, Interface between bone tissue and implants of solid hydroxyapatite or hydroxyapatite-coated titanium implants, Biomaterials 10 (1989) 121–125. https://doi.org/10.1016/0142-9612(89)90044-6.
[80] H. Bluthmann, Chromatography of histones on hydroxyapatite columns, J. Chromatogr. A 137 (1977) 222–227. https://doi.org/10.1016/S0021-9673(00)89262-6.
[81] A. Haider, K.C. Gupta, I.K. Kang, PLGA/nHA hybrid nanofiber scaffold as a nanocargo carrier of insulin for accelerating bone tissue regeneration, Nanoscale Res. Lett. 9 (2014) 314. https://doi.org/10.1186/1556-276X-9-314.
[82] F.J. Martínez-Vázquez, M.V. Cabañas, J.L. Paris, D. Lozano, M. Vallet-Regí, Fabrication of novel Si-doped hydroxyapatite/gelatine scaffolds by rapid prototyping for drug delivery and bone regeneration, Acta Biomater. 15 (2015) 200–209. https://doi.org/10.1016/j.actbio.2014.12.021.
[83] Z.J. Rong, L.J. Yang, B.T. Cai, L.X. Zhu, Y.L. Cao, G.F. Wu, et al., Porous nanohydroxyapatite/collagen scaffold containing drug-loaded ADM–PLGA microspheres for bone cancer treatment, J. Mater. Sci. Mater. Med. 27 (2016) 89–101. https://doi.org/10.1007/s10856-016-5699-0.
[84] D. Li, X. Huang, Y. Wu, J. Li, W. Cheng, J. He, et al., Preparation of pH-responsive mesoporous hydroxyapatite nanoparticles for intracellular controlled release of an anticancer drug, Biomater. Sci. 4 (2016) 272–280. https://doi.org/10.1039/C5BM00228A.
[85] H. Xiong, S. Du, J. Ni, J. Zhou, J. Yao, Mitochondria and nuclei dual-targeted heterogeneous hydroxyapatite nanoparticles for enhancing therapeutic efficacy of doxorubicin, Biomaterials 94 (2016) 70–83. https://doi.org/10.1016/j.biomaterials.2016.04.004.
[86] M. Öner, E. Yetiz, E. Ay, U. Uysal, Ibuprofen release from porous hydroxyapatite tablets, Ceram. Int. 37 (2011) 2117–2125. https://doi.org/10.1016/j.ceramint.2011.02.021.
[87] F. Shao, L. Liu, K. Fan, Y. Cai, J. Yao, Ibuprofen loaded porous calcium phosphate nanospheres for skeletal drug delivery system, J. Mater. Sci. 47 (2012) 1054–1058. https://doi.org/10.1007/s10853-011-5894-9.
[88] S. Li, K. Wang, K.C.A. Chang, M. Zong, J. Wang, Y.G. Cao, et al., Preparation and evaluation of nano-hydroxyapatite/poly(styrene-divinylbenzene) porous microspheres for aspirin carrier, Sci. China Chem. 55 (2012) 1134–1139. https://doi.org/10.1007/s11426-012-4519-8.
[89] H. Aghaei, A.A. Nourbakhsh, S. Karbasi, R.J. Kalbasi, M. Rafienia, N. Nourbakhsh, et al., Investigation on bioactivity and cytotoxicity of mesoporous nanocomposite MCM-48/hydroxyapatite

for ibuprofen drug delivery, Ceram. Int. 40 (2014) 7355–7362. https://doi.org/10.1016/j.ceramint.2013.12.079.
[90] A. Ilie, C. Ghiţulică, E. Andronescu, A. Cucuruz, A. Ficai, New composite materials based on alginate and hydroxyapatite as potential carriers for ascorbic acid, Int. J. Pharm. 510 (2016) 501–507. https://doi.org/10.1016/j.ijpharm.2016.01.025.
[91] E. Kolanthai, K. Ganesan, M. Epple, S.N. Kalkuraa, Synthesis of nanosized hydroxyapatite/agarose powders for bone filler and drug delivery applications, Mater. Today Commun. 8 (2016) 31–40. https://doi.org/10.1016/j.mtcomm.2016.03.008.
[92] W. He, L. Pan, Y. Wang, F.C. Meldrum, Bioinspired synthesis of large-pore, mesoporous hydroxyapatite nanocrystals for the controlled release of large pharmaceutics, Cryst. Growth Des. 15 (2015) 723–731. https://doi.org/10.1021/cg501515c.
[93] A. Szcześ, L. Hołysz, E. Chibowski, Synthesis of hydroxyapatite for biomedical applications, Adv. Colloid Interface Sci. 249 (2017) 321–330. https://doi.org/10.1016/j.cis.2017.04.007.
[94] A.R. Ibrahim, X. Li, Y. Zhou, Y. Huang, W. Chen, H. Wang, J. Li, Synthesis of spongy-like mesoporous hydroxyapatite from raw waste eggshells for enhanced dissolution of ibuprofen loaded via supercritical CO_2, Int. J. Mol. Sci. 16 (2015) 7960. https://doi.org/10.3390/ijms16047960.
[95] A. Liu, G.H. Xue, M. Sun, H.F. Shao, C.Y. Ma, Q. Gao, Z.R. Gou, S.G. Yan, Y.M. Liu, Y. He, 3D printing surgical implants at the clinic: an experimental study on anterior cruciate ligament reconstruction, Sci. Rep. 6 (2016) 21704. https://doi.org/10.1038/srep21704.
[96] A.E. Jakus, A.L. Rutz, R.N. Shah, Advancing the field of 3D biomaterial printing, Biomed. Mater. 11 (2016) 014102. https://doi.org/10.1088/1748-6041/11/1/014102.
[97] S. Ohba, R. Shido, I. Asahina, Application of hydroxyapatite/collagen composite material for maxillary sinus floor augmentation, J. Oral Sci. 63 (2021) 295–297. https://doi.org/10.2334/josnusd.21-0163.
[98] M.Y. Shaheen, Nanocrystalline hydroxyapatite in periodontal bone regeneration: A systematic review, Saudi Dent. J. 34 (2022) 647–660. https://doi.org/10.1016/j.sdentj.2022.09.005.
[99] M. Kamboj, R. Arora, H. Gupta, Comparative evaluation of the efficacy of synthetic nanocrystalline hydroxyapatite bone graft (Ostim®) and synthetic microcrystalline hydroxyapatite bone graft (Osteogen®) in the treatment of human periodontal intrabony defects: A clinical and Denta scan study, J. Indian Soc. Periodontol. 20 (2016) 423–428. https://doi.org/10.4103/0972-124X.184036.
[100] A. Szcześ, L. Hołysz, E. Chibowski, Synthesis of hydroxyapatite for biomedical applications, Adv. Colloid Interface Sci. 249 (2017) 321–330. https://doi.org/10.1016/j.cis.2017.04.007.
[101] P. Kumar, B.S. Dehiya, A. Sindhu, Bioceramics for hard tissue engineering applications: A review, Int. J. Appl. Eng. Res. 13 (2018) 2744–2752.
[102] H. Tschernitschek, L. Borchers, W. Geurtsen, Nonalloyed titanium as a bioinert metal: A review, J. Prosthet. Dent. 96 (2006) 12. https://doi.org/10.1016/j.prosdent.2006.02.020.
[103] C. Montoya, Y. Du, A.L. Gianforcaro, S. Orrego, M. Yang, P.I. Lelkes, On the road to smart biomaterials for bone research: Definitions, concepts, advances, and outlook, Bone Res. 9 (2021) 12. https://doi.org/10.1038/s41413-020-00131-z.
[104] S. Sonarkar, R. Purba, Bioactive materials in conservative dentistry, Int. J. Contemp. Dent. Med. Rev. (2015). https://doi.org/10.15713/ins.ijcdmr.47.

[105] S. Nour, N. Baheiraei, R. Imani, N. Rabiee, M. Khodaei, A. Alizadeh, S.M. Moazzeni, Bioactive materials: A comprehensive review on interactions with the biological microenvironment based on the immune response, J. Bionic Eng. 16 (2019) 563–581. https://doi.org/10.1007/s42235-019-0046-z.
[106] A. Pandey, S. Midha, R.K. Sharma, R. Maurya, V.K. Nigam, S. Ghosh, K. Balani, Antioxidant and antibacterial hydroxyapatite-based biocomposite for orthopedic applications, Mater. Sci. Eng. C 88 (2018) 13–24. https://doi.org/10.1016/j.msec.2018.02.014.
[107] T.W. Bauer, S.T. Smith, Bioactive materials in orthopaedic surgery: Overview and regulatory considerations, Clin. Orthop. Relat. Res. 395 (2002) 11–22.
[108] T. Liu, K. Huang, L. Li, Z. Gu, X. Liu, X. Peng, T. Kuang, High performance high-density polyethylene/hydroxyapatite nanocomposites for load-bearing bone substitute: Fabrication, in vitro and in vivo biocompatibility evaluation, Compos. Sci. Technol. 175 (2019) 100–110. https://doi.org/10.1016/j.compscitech.2019.03.012.
[109] J.W. Park, J.U. Hwang, J.H. Back, S.W. Jang, H.J. Kim, P.S. Kim, S. Shin, High strength PLGA/hydroxyapatite composites with tunable surface structure using PLGA direct grafting method for orthopedic implants, Compos. B Eng. 178 (2019) 107449. https://doi.org/10.1016/j.compositesb.2019.107449.
[110] H. Oonishi, Orthopaedic applications of hydroxyapatite, Biomaterials 12 (1991) 171–178. https://doi.org/10.1016/0142-9612(91)90196-H.
[111] Y. Ito, H. Hasuda, M. Kamitakahara, C. Ohtsuki, M. Tanihara, I.K. Kang, O.H. Kwon, A composite of hydroxyapatite with electrospun biodegradable nanofibers as a tissue engineering material, J. Biosci. Bioeng. 100 (2005) 43–49. https://doi.org/10.1263/jbb.100.43.
[112] J. Venugopal, P. Vadagama, T.S. Sampath Kumar, S. Ramakrishna, Biocomposite nanofibres and osteoblasts for bone tissue engineering, Nanotechnology 18 (2007) 055101. https://doi.org/10.1088/0957-4484/18/5/055101.
[113] J. Venugopal, S. Low, A.T. Choon, A.B. Kumar, S. Ramakrishna, Electrospun-modified nanofibrous scaffolds for the mineralization of osteoblast cells, J. Biomed. Mater. Res. A 85 (2008) 408–417. https://doi.org/10.1002/jbm.a.31538.
[114] J. Venugopal, S. Low, A.T. Choon, A.B. Kumar, S. Ramakrishna, Nanobioengineered electrospun composite nanofibers and osteoblasts for bone regeneration, Artif. Organs 32 (2008) 388–397. https://doi.org/10.1111/j.1525-1594.2008.00557.x.
[115] M.P. Prabhakaran, J. Venugopal, S. Ramakrishna, Electrospun nanostructured scaffolds for bone tissue engineering, Acta Biomater. 5 (2009) 2884–2893. https://doi.org/10.1016/j.actbio.2009.05.007.
[116] L.L. Hench, Sol–gel materials for bioceramic applications, State Mater. Sci. 2 (2017) 604–610. https://doi.org/10.1016/S1359-0286(97)80053-8.
[117] T.J. Matsumoto, S.H. An, T. Ishimoto, T. Nakano, T. Matsumoto, S. Imazato, Zirconia–hydroxyapatite composite material with microporous structure, Dent. Mater. 27 (2011) e205–e212. https://doi.org/10.1016/j.dental.2011.05.012.
[118] B. Bulut, Z. Erkmen, E. Kayali, Biocompatibility of hydroxyapatite–alumina and hydroxyapatite–zirconia composites including commercial inert glass (CIG) as a ternary component, J. Ceram. Sci. Technol. 7 (2016) 263–276. https://doi.org/10.4416/JCST2016-00011.

[119] V. Chopra, J. Thomas, A. Sharma, G. Bhardwaj, H.S. Sohal, A. Gohain, et al., [Title Missing], ACS Biomater. Sci. Eng. 6 (2020) 6710–6725. https://doi.org/10.1021/acsbiomaterials.0c00370.
[120] U. Joos, H.P. Wiesmann, J. Neunzehn, U. Meyer, Applications of biomaterials in alveolar and maxillofacial bone reconstruction, in: Preprosthetic Maxillofac. Surg., 2011, pp. 175–184. https://doi.org/10.1533/9780857092427.2.175.
[121] A.E. Porter, P. Taak, L.W. Hobbs, M.J. Coathup, G.W. Blunn, M. Spector, Bone bonding to hydroxyapatite and titanium surfaces on femoral stems retrieved from human subjects at autopsy, Biomaterials 25 (2004) 5199–5208. https://doi.org/10.1016/j.biomaterials.2003.12.018.
[122] S. Mohammadi Nejad, H. Özgüneş, N. Başaran, Pharmacological and toxicological properties of eugenol, Turk. J. Pharm. Sci. 14 (2017) 201–206. https://doi.org/10.4274/tjps.62207.
[123] K.G. Lee, T. Shibamoto, Antioxidant property of aroma extract isolated from clove buds [Syzygium aromaticum (L.) Merr. et Perry], Food Chem. 74 (2001) 443–448. https://doi.org/10.1016/S0308-8146(01)00161-3.
[124] D.G. Barceloux, Medical Toxicology of Natural Substances: Foods, Fungi, Medicinal Herbs, Plants and Venomous Animals, Wiley, 2008, pp. 437–442. https://doi.org/10.1002/9780470330319.ch59.
[125] P. Tammannavar, C. Pushpalatha, S. Jain, S.V. Sowmya, An unexpected positive hypersensitive reaction to eugenol, Case Rep. (2013) bcr2013009464. https://doi.org/10.1136/bcr-2013-009464.
[126] A. Marchese, R. Barbieri, E. Coppo, I.E. Orhan, M. Daglia, S.F. Nabavi, M. Izadi, M. Abdollahi, S.M. Nabavi, M. Ajami, Antimicrobial activity of eugenol and essential oils containing eugenol: A mechanistic viewpoint, Crit. Rev. Microbiol. 43 (2017) 668–689. https://doi.org/10.1080/1040841X.2017.1295225.
[127] B. Pavithra, Eugenol: A review, J. Pharm. Sci. Res. 6 (2014) 153–154.
[128] S. Abbaszadeh, A. Sharifzadeh, H. Shokri, et al., Antifungal efficacy of thymol, carvacrol, eugenol and menthol as alternative agents to control the growth of food-relevant fungi, J. Mycol. Med. 24 (2014) e51–e56. https://doi.org/10.1016/j.mycmed.2014.01.063.
[129] A. Sharma, G. Bhardwaj, H.S. Sohal, A. Gohain, Chapter 9 – Eugenol, in: J. Kour, G.A. Nayik (Eds.), Nutraceuticals Health Care, Academic Press, 2022, pp. 177–198. https://doi.org/10.1016/B978-0-323-89779-2.00007-7.
[130] G.E. Batiha, L.M. Alkazmi, L.G. Wasef, A.M. Beshbishy, E.H. Nadwa, E.K. Rashwan, Syzygium aromaticum L. (Myrtaceae): Traditional uses, bioactive chemical constituents, pharmacological and toxicological activities, Biomolecules 10 (2020) 202. https://doi.org/10.3390/biom10020202.
[131] A.N. Daniel, S.M. Sartoretto, G. Schmidt, S.M. Caparroz-Assef, C.A. Bersani-Amado, R.K.N. Cuman, Anti-inflammatory and antinociceptive activities of eugenol essential oil in experimental animal models, Rev. Bras. Farmacogn. 19 (2009) 212–217. https://doi.org/10.1590/S0102-695X2009000200006.
[132] F.F.M. Da Silva, F.J.Q. Monte, T.L.G. de Lemos, P.G. Garcia do Nascimento, A.K. de Medeiros Costa, L.M.M. de Paiva, Eugenol derivatives: Synthesis, characterization, and evaluation of antibacterial and antioxidant activities, Chem. Cent. J. 12 (2018) 34. https://doi.org/10.1186/s13065-018-0407-4.

[133] N.B.A. Prasetya, et al., [Title Missing], IOP Conf. Ser. Mater. Sci. Eng. 509 (2019) 012101. https://doi.org/10.1088/1757-899X/509/1/012101.
[134] N. Ngadiwiyana, R.D. Soelistyowati, H. Sastrohamidjojo, Dimerisasi metilisoeugenol dengan katalis HCl, J. Kim. Sains Apl. 5 (2002) 1–6. https://doi.org/10.14710/jgi.%25v.%25i.%25p.
[135] M. Yuwono, Siswandono, A.F. Hafid, A.T. Poernomo, M. Agil, G. Indrayanto, S. Ebel, Eugenol, in: H.G. Brittain (Ed.), Anal. Profiles Drug Subst. Excipients, Vol. 29, Academic Press, 2002, pp. 149–177. https://doi.org/10.1016/S1075-6280(02)29006-0.
[136] M. Schmid-Schwap, A. Franz, F. Konig, M. Bristela, T. Lucas, E. Piehslinger, et al., Cytotoxicity of four categories of dental cements, Dent. Mater. 25 (2009) 360–368. https://doi.org/10.1016/j.dental.2009.01.022.
[137] K.D. Jandt, B.W. Sigusch, Future perspectives of resin-based dental materials, Dent. Mater. 25 (2009) 1001–1006. https://doi.org/10.1016/j.dental.2009.02.009.
[138] K. Pramod, S.H. Ansari, J. Ali, Eugenol: A natural compound with versatile pharmacological actions, Nat. Prod. Commun. 5 (2010) 1999–2006. https://doi.org/10.1177/1934578X1000501236.
[139] A. Martínez-Herrera, A. Pozos-Guillén, S. Ruiz-Rodríguez, A. Garrocho-Rangel, Effect of 4-allyl-1-hydroxy-2-methoxy-benzene (eugenol) on inflammatory and apoptosis processes in dental pulp fibroblasts, Mediators Inflamm. (2016) 9371403. https://doi.org/10.1155/2016/9371403.
[140] W. Steiling, M. Bracher, P. Courtellemont, O. de Silva, The HET-CAM, a useful in vitro assay for assessing the eye irritation properties of cosmetic formulations and ingredients, Toxicol. In Vitro 13 (1999) 375–384. https://doi.org/10.1016/S0887-2333(98)00091-5.
[141] D.A. Surducan, R.C. Racea, M. Cabuta, I. Olariu, I. Macasoi, L.C. Rusu, S.D. Chiriac, D. Chioran, S. Dinu, M.O. Pricop, Eugenol induces apoptosis in tongue squamous carcinoma cells by mediating the expression of Bcl-2 family proteins, Life (Basel) 13 (2022) 22. https://doi.org/10.3390/life13010022.
[142] P. Sen, Therapeutic potentials of Tulsi: From experience to facts, Drugs News Views 1 (1993) 15–21.
[143] S.M. Hwang, K. Lee, S.T. Im, E.J. Go, C.K. Park, Co-application of eugenol and QX-314 elicits the prolonged blockade of voltage-gated sodium channels in nociceptive trigeminal ganglion neurons, Biomolecules 10 (2020) 1513. https://doi.org/10.3390/biom10111513.
[144] D.S. Goswami, Permeation enhancer for TDDS from natural and synthetic sources: A review, J. Biomed. Pharm. Res. 2 (2013) 19–29.
[145] W.P. Saunders, E.M. Saunders, Coronal leakage as a cause of failure in root-canal therapy: A review, Dent. Traumatol. 10 (1994) 105–108. https://doi.org/10.1111/j.1600-9657.1994.tb00533.x.
[146] M. Torabinejad, B. Ung, J.D. Kettering, In vitro bacterial penetration of coronally unsealed endodontically treated teeth, J. Endod. 16 (1990) 566–569. https://doi.org/10.1016/S0099-2399(07)80198-1.
[147] A. Khayat, S.J. Lee, M. Torabinejad, Human saliva penetration of coronally unsealed obturated root canals, J. Endod. 19 (1993) 458–461. https://doi.org/10.1016/S0099-2399(06)80533-9.
[148] J.A. Guerra, J.E. Skribner, L.M. Lin, Influence of a base on coronal microleakage of post-prepared teeth, J. Endod. 20 (1994) 589–591. https://doi.org/10.1016/S0099-2399(06)80082-8.
[149] R. De Moor, G. Hommez, The importance of apical and coronal leakage in the success or failure of endodontic treatment, Rev. Belg. Med. Dent. 55 (2000) 334–344.

[150] M. Gimbel, A. Correa, Calcium hydroxide as a temporary filling of the post space in root-filled teeth, Oral Surg. Oral Med. Oral Pathol. Oral Radiol. Endod. 94 (2002) 98–102. https://doi.org/10.1067/moe.2002.123865.
[151] A. Marchese, R. Barbieri, E. Coppo, et al., Antimicrobial activity of eugenol and essential oils containing eugenol: A mechanistic viewpoint, Crit. Rev. Microbiol. 43 (2017) 668–689. https://doi.org/10.1080/1040841X.2017.1295225.
[152] N. Ahmad, F.J. Ahmad, S. Bedi, S. Sharma, S. Umar, M.A. Ansari, A novel nanoformulation development of eugenol and their treatment in inflammation and periodontitis, Saudi Pharm. J. 27 (2019) 778–790. https://doi.org/10.1016/j.jsps.2019.04.014.
[153] F.J. Navarro Triviño, C. Barrales, R. Ruiz-Villaverde, Eugenol allergy mimicking aphthous oral recurrent and burning mouth syndrome, Contact Dermatitis (2019) 1–2. https://doi.org/10.1111/cod.13365.
[154] D.L.J. Opdyke, Monographs on fragrance raw materials, Elsevier, 1979, pp. 247–249, 376. https://doi.org/10.1016/B978-0-08-023775-6.50182-X.
[155] R. Žalnėravičius, V. Klimas, A. Paškevičius, G. Grincienė, R. Karpicz, A. Jagminas, A. Ramanavičius, Highly efficient antimicrobial agents based on sulfur-enriched, hydrophilic molybdenum disulfide nano/microparticles and coatings functionalized with palladium nanoparticles, J. Colloid Interface Sci. 591 (2021) 115–128. https://doi.org/10.1016/j.jcis.2021.01.103.
[156] E. Bajorinaite, L. Michailova, S. Jureviciute, D. Sokol, Z. Stankeviciute, I. Grigoraviciute, A. Kareiva, Initial evaluation of waste phosphogypsum for its use as a precursor for bioceramic materials, Chemija 35 (2024) 35–44. https://doi.org/10.6001/chemija.2024.35.2.2.
[157] K. Ishikawa, E. Garskaite, A. Kareiva, Sol-gel synthesis of calcium phosphate-based biomaterials—A review of environmentally benign, simple and effective synthesis routes, J. Sol-Gel Sci. Technol. 94 (2020) 551–572. https://doi.org/10.1007/s10971-020-05245-8.
[158] I. Grigoraviciute-Puroniene, Y. Tanaka, V. Vegelyte, Y. Nishimoto, K. Ishikawa, A. Kareiva, A novel synthetic approach to low-crystallinity calcium deficient hydroxyapatite, Ceram. Int. 45 (2019) 15620–15623. https://doi.org/10.1016/j.ceramint.2019.05.072.
[159] B.Z. Chowdhry, J.P. Ryall, T.J. Dines, A.P. Mendham, Infrared and Raman spectroscopy of eugenol, isoeugenol, and methyl eugenol: Conformational analysis and vibrational assignments from density functional theory calculations of the anharmonic fundamentals, J. Phys. Chem. A 119 (2015) 11280–11292. https://doi.org/10.1021/acs.jpca.5b07607.
[160] M.S. Djosic, V.B. Miskovic-Stankovic, S. Milonjic, Z.M. Kacarevic-Popovic, N. Bibic, J. Stojanovic, Electrochemical synthesis and characterization of hydroxyapatite powders, Mater. Chem. Phys. 111 (2008) 137–142. https://doi.org/10.1016/j.matchemphys.2008.03.045.
[161] I. Grigoraviciute-Puroniene, K. Tsuru, E. Garskaite, Z. Stankeviciute, A. Beganskiene, K. Ishikawa, A. Kareiva, A novel wet polymeric precipitation synthesis method for monophasic β-TCP, Adv. Powder Technol. 28 (2017) 2325–2331. https://doi.org/10.1016/j.apt.2017.06.014.
[162] S.M. Huang, S.M. Liu, W.C. Chen, C.L. Ko, C.J. Shih, J.C. Chen, Morphological changes, antibacterial activity, and cytotoxicity characterization of hydrothermally synthesized metal ions-incorporated nanoapatites for biomedical application, Pharmaceuticals 15 (2022) 885. https://doi.org/10.3390/ph15070885.

[163] K. Markowitz, M. Moynihan, M. Liu, S. Kim, Biologic properties of eugenol and zinc oxide-eugenol: A clinically oriented review, Oral Surg. Oral Med. Oral Pathol. 73 (1992) 729–737. https://doi.org/10.1016/0030-4220(92)90020-Q.